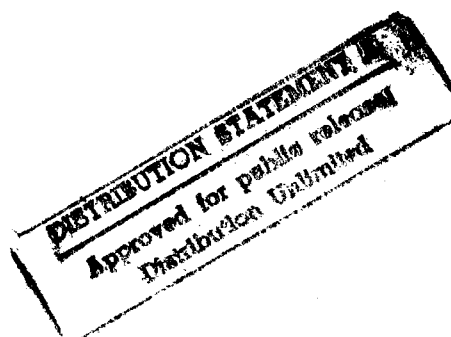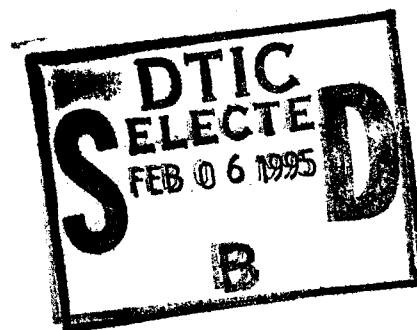# Dynamics of a Split Torque Helicopter Transmission

Timothy L. Krantz
Vehicle Propulsion Directorate
U. S. Army Research Laboratory
Lewis Research Center
Cleveland, Ohio

DTIC
SELECTED
FEB 0 6 1995
B

DISTRIBUTION STATEMENT
Approved for public release
Distribution Unlimited

June 1994

NASA

National Aeronautics and
Space Administration

U.S. ARMY

ARL

RESEARCH LABORATORY

CONTENTS

DYNAMICS OF A SPLIT TORQUE HELICOPTER TRANSMISSION

Timothy L. Krantz
National Aeronautics and Space Administration
Lewis Research Center
Cleveland, Ohio 44135

Summary

Split torque designs, proposed as alternatives to traditional planetary designs for helicopter main rotor transmissions, can save weight and be more reliable than traditional designs. This report presents the results of an analytical study of the system dynamics and performance of a split torque gearbox that uses a balance beam mechanism for load sharing. The Lagrange method was applied to develop a system of equations of motion. The mathematical model includes time-varying gear mesh stiffness, friction, and manufacturing errors. Cornell's method for calculating the stiffness of spur gear teeth was extended and applied to helical gears. The phenomenon of sidebands spaced at shaft frequencies about gear mesh fundamental frequencies was simulated by modeling total composite gear errors as sinusoid functions. Although the gearbox has symmetric geometry, the loads and motions of the two power paths differ. Friction must be considered to properly evaluate the balance beam mechanism. For the design studied, the balance beam is not an effective device for load sharing unless the coefficient of friction is less than 0.003. The complete system stiffness as represented by the stiffness matrix used in this analysis must be considered to precisely determine the optimal tooth indexing position.

Symbols

[A]   rotational coordinate transformation matrix

B   energy dissipation function

C   damping coefficient

D   rotation due to deflection

$\bar{E}$ mean value of displacement element function

e   displacement element length

F   friction force

I   inertia

K   stiffness

[K]   stiffness matrix

$\bar{K}$ mean value of stiffness

L   Lagrangian

M   mass or inertia

Q   generalized force

q   generalized coordinate

r   gear base radius

T   dimensionless time

T total kinetic energy

t   time

U   unit torque

V   total potential energy

X,Y,Z   Cartesian coordinates

$\cdot$ first time derivative

$\cdot\cdot$ second time derivative

α_k angles defining locations of shafts (k = 1, 2, p, and B)

β helix angle of helical gears

ζ damping ratio

θ rotational speed of component

μ coefficient of friction

ϕ phase angle of time-varying functions

ψ	angular displacement of gears
ω	input shaft speed

Subscripts:

a	axial
B	bull gear
b	bearing
bal	balance beam
i	input energy source
j	counter subscript for generalized coordinates (j = 1,2,3,...,18)
m	tooth mesh
o	output load
p	pinion
s	shaft
sB	shaft between bull gear and output load
sp	shaft between pinion and input energy source
s1,s2	shaft between spur and helical gear of first and second compound gears
xxbB	bearing of bull gear in X-direction
xxbp	bearing of pinion gear in X-direction
xxb1,xxb2	bearing of first, second compound gears in X-direction
yybB	bearing of bull gear in Y-direction
yybp	bearing of pinion gear in Y-direction
yyb1,yyb2	bearing of first and second compound gears in Y-direction
zp	axial direction of pinion
z1,z2	axial direction of first, second compound gears
1,2	first and second compound gears
1h,2h	first and second helical gears
1mh,2mh	first and second helical mesh (pinion and compound gears)
1s,2s	first and second spur mesh (compound and bull gears)

Chapter 1

Introduction

1.0 Background

The requirements for the drive systems of helicopters and other aircraft are especially demanding. The engine supplies the power at high speed whereas the rotor must operate at low speed. The drive system transmits the engine power to the rotor while providing a speed reduction that, for helicopters, is typically 100 to 1. Also, the weight, mechanical efficiency, vibration characteristics, and reliability of the drive system all have a significant impact on the overall performance of the vehicle. The weight of the drive system is an especially important factor. As a result of analysis, experimentation, and field experience, rotorcraft transmissions have evolved to provide a high degree of performance. However, further improvements in performance are desired. The next generation of rotorcraft will require lighter, quieter, and more reliable drive systems to increase the vehicle payload, improve performance and readiness, provide greater passenger comfort and safety, and lower operating costs.

The configuration of the main rotor gearbox is one of the most important characteristics of a helicopter's drive system. The most common and conventional configuration for the final gear stage of a main rotor gearbox is a planetary stage which has an output shaft driven by several planets. This configuration permits the division of the transmitted torque among several planets. This division results in a gearbox that is lighter compared with a parallel shaft gearbox in which each gear transmits the entire torque. An alternative to the conventional planetary stage is a split torque stage. A split torque design is a parallel shaft arrangement that, similar to a planetary stage, transfers power to the output shaft through multiple pinions. This arrangement shares the torque-splitting advantage of a planetary stage, and it also can have a larger reduction ratio than is possible for a planetary design. A large reduction ratio at the final gear stage tends to reduce the overall transmission weight. Researchers developing the designs and technology for future rotorcraft transmissions have considered using a split torque stage and, in some cases, have chosen designs using split torque stages as the most promising configuration (refs. 1 to 3). One design proposed for a split torque stage helicopter application is shown in figure 1.1. White (ref. 4) states that this split torque stage not only offers an overall weight reduction, but also promises the following advantages when compared with a conventional planetary design:

(1) High ratio of speed reduction at final stage
(2) Reduced number of gear stages
(3) Lower energy losses
(4) Increased reliability of separate drive paths
(5) Fewer number of gears and bearings
(6) Lower noise levels from gear meshes

Thus, there is sufficient justification to pursue the development of a new generation of helicopter transmissions that include a split torque stage.

Split torque configurations for aircraft have had limited production applications. A split torque design for a helicopter main rotor gearbox was developed by Westland Helicopters (ref. 5), and another design is used in the Russian Mi-26 heavy lift helicopter (ref. 6). Although not known by the name split torque, similar configurations are also used in marine gearboxes (ref. 7). Many different split torque gearbox conceptual designs have been proposed (refs. 1 to 13). An aspect of all the split torque designs that must be addressed by the designer is the equality of the torque split. Because of manufacturing errors, one of the two power paths might carry much more than half of the total power path unless some effective load-sharing method is employed. Since each

4

power path must be sized to carry the maximum possible load, the weight of the transmission will be minimized only if the equality of the torque split can be guaranteed. One method to control this equality is to specify and maintain very precise manufacturing tolerances. This is a feasible option for today's manufacturing capabilities but may not be the optimal solution. Other methods have been proposed, including axially floating shafts, torsionally compliant shafts, balancing mechanisms, and laterally compliant bearing supports. These methods may significantly alter the vibration properties and performance of the gearbox. The performance of a split torque design depends heavily on the method selected to achieve torque splitting. The purpose of this work was to develop and apply a dynamic analysis for split torque transmissions, with an emphasis on load sharing.

1.1   Scope and Approach

The focus of this work was to study one particular split torque gearbox configuration (fig. 1.1) that was proposed by White (ref. 4) for a helicopter main rotor transmission. The emphasis was to evaluate the system dynamics and especially the torque sharing between the two parallel power paths. The results can be used to gain an understanding of the characteristics of this particular split torque design. Also, the mathematical model that was developed can be adapted to analyze and optimize other geared systems using split torque arrangements.

The remainder of this report is divided into three sections. Chapter 2 describes both the methods used to develop a mathematical model for studying split torque gearbox arrangements and those used by others to model geared systems. The assumptions made and methods used to develop the mathematical model are described. A set of equations is derived to describe the loads and motions of the gearbox. Special considerations unique to modeling split torque arrangements are discussed. The methods used to make the equations of motion non-dimensional are described along with solution techniques for the computer simulation of gearbox motions.

Chapter 3 describes new techniques developed and used to model closed-loop test facilities, helical gear mesh stiffnesses, and gear manufacturing errors. Both static and dynamic analytical solutions were obtained for the mathematical model. The solutions are discussed to describe the effects of friction, bearing stiffness, and manufacturing errors on the system's performance. Chapter 4 presents a summary and the conclusions drawn from this work.

Chapter 2

Mathematical Modeling

2.0 Review of Gear Dynamics Modeling

Many researchers have studied the analytical simulation of geared system dynamics. A great number of mathematical models, analytical methods, and computer codes have been developed. A representative sampling of these methods can be found in references 14 to 25. The proper approach and the complexity of the mathematical model depend on both the characteristics of the system being simulated and on the phenomena being investigated.

A representative model used to study gear dynamics (fig. 2.1) consists of two rigidly mounted disks. The rotational displacements of these two disks are coupled by three elements located along a line tangent to both disks. These three, a spring, a damper, and a displacement element, are used to model the meshing gear teeth. Much work has been done to study how to assign the proper characteristics to these three elements to simulate either a typical or a particular pair of gears (e.g., refs. 26 to 28). The spring stores potential energy. Most researchers use a time-varying function to define the spring stiffness. The function approximates the stiffness change that occurs when the number of gear teeth in contact changes as the gears rotate. The damper dissipates energy and is often defined as a proportional damper. Therefore, its characteristics change with time since it is proportional to the time-varying mesh stiffness. The displacement element can be thought of as a massless, rigid link whose length changes as a function of the angular positions of the pinion and gear. It is included in the model for simulating the phenomenon of transmission error and is often defined as a function of time.

A pair of gears with infinitely rigid teeth and perfect involute profiles transmits exactly uniform angular motion. Any real gear pair deviates from transmitting uniform angular motion, and this deviation is called the dynamic transmission error. A real gear pair deviates from transmitting uniform motion because of the compliance of the gear teeth, effects of inertia, and deviations of the actual contacting surfaces of the loaded teeth from conjugate surfaces. These deviations can include intentional profile modifications, manufacturing errors, and deflections of the gear body and supports. Considered the main source of vibration excitation in many geared systems, the loaded static transmission error is the error of a loaded gear pair rotating at a very slow speed and, therefore, rotating with no inertia effects. The relative contributions of the various components of the loaded static transmission error (i.e., varying stiffness, manufacturing errors, support deflection) depend on the gear design, tooth profile modifications, the manufacturing quality, the torque level being transmitted, and the mechanical properties of other system components. Similarly, defining the stiffness, damping, and displacement elements of a gear mesh model depends on the system and the phenomena being studied. For example, some researchers (refs. 23 and 24) have used a constant mesh stiffness and an appropriate definition of the displacement element and were able to successfully simulate the motions of real systems. However, this method may not be appropriate for all gear systems and analyses.

Gear pairs are only components of a larger mechanical system. Input and output inertias connected to the gears through torsionally compliant shafts are often included in gear dynamics models. For many real systems that have relatively compliant shafts and bearing mounts, the torsional and lateral motions are strongly coupled. To simulate this phenomenon, the lateral stiffness of the gear mounts must be included in the model. Gear systems with multiple stages (ref. 16) and planetary arrangements (refs. 29 to 32) have also been modeled and studied.

A recent study of a split torque helicopter transmission is that of D. Hochmann, D. Houser, and J. Thomas (ref. 33). They analyzed the load distribution of spur and double helical gear pairs used in a split torque helicopter

transmission. They suggested that, by altering the gear tooth profile modifications and by staggering the phasing of the double helical gear mesh used in the design, the loaded static transmission error could be reduced without seriously degrading load distribution on the gear teeth.

Another aspect of split torque configurations that has not been rigorously studied is the overall dynamic behavior. A special characteristic of split torque drivetrains is the use of some method to guarantee that the power be split evenly between the parallel paths. Several different methods have been proposed (refs. 1 to 13). Rashidi and Krantz (ref. 34) developed a mathematical model to study these power-splitting or load-sharing methods and to study the system dynamics of the resulting design. One of the main objectives of this work was to apply the mathematical model to simulate the motions and loads of the split torque test rig at the NASA Lewis Research Center. The remainder of this chapter describes the analytical method and solution techniques. The application of the model is described in chapter 3.

2.1   Description of the Design

The transmission design under study, a cooperative effort of the U.S. Army and the NASA Lewis Research Center, is a split torque gearbox proposed and developed by G. White (ref. 4) under an Army-NASA contract to approximate the power requirement and match the speed reduction requirement of a version of the U.S. Army's OH–58 helicopter main rotor transmission. The final two gear stages of the split torque test gearbox are shown in figure 2.2. This design relies on the positioning of helical gears by a self-adjusting mechanism to obtain load sharing. A main rotor transmission using this concept was projected to be 25 percent lighter than a conventional design using a planetary output stage.

A split torque test gearbox using this design was built to research split torque concepts. The rated input power to the test gearbox is 373 kW (500 hp) at 8780 rpm. The input power is carried through the input helical pinion and is split between two helical gears at the first reduction stage. The power is combined at the second and final reduction stage. Two spur pinions drive the output bull gear at 347.5 rpm. Thrust loads are produced at each of the two helical meshes. These loads are reacted through a pivoted balance beam. The beam acts to balance the power carried by each shaft by coupling the axial positions of the two gear/pinion assemblies. The concept of this design is that the thrust loads act to adjust the axial positions of the two gear/pinion assemblies such that the power is split evenly between the two power paths.

One of the main objectives of this work was to develop a mathematical model that could be used to identify and study the effect of design parameters on the overall dynamic behavior of the system. For example, the angles between the centerlines of the gears (identified in fig. 2.3) were considered a possible significant parameter. These angles influence the stiffness properties of the system and, for a given set of gears, define the relative phasing of the time-varying mesh stiffnesses. It was also desirable to study the effect of a subcomponent's mechanical properties on the system performance; thus, the analytical method was chosen and applied with these objectives in mind. The following important properties that can be simulated by the model are categorized as

(1)   Microgeometric parameters such as tooth profile geometry, shaft hub eccentricities, and tooth spacing and lead errors

(2)   Macrogeometric parameters such as gear mesh pitch and pressure angles, the helix angle of the helical mesh, and shaft and bearing locations

(3)   Component material properties and bulk dimensions that define the inertia, stiffness, and dampening properties of the components

(4)   Type and geometry of the bearings that support the gear shafts

2.2 Analytical Model

The split torque transmission design shown in figure 2.2 was modeled by a set of inertia, stiffness, damping, and displacement elements. The analytical model is shown in figure 2.4 with the gear/pinion assemblies termed as compound gears. Along with the inertia and stiffness elements shown, the model also includes a damping element parallel to each stiffness element, an input inertia, and an output inertia. Displacement elements are also included at the gear mesh locations as illustrated in figure 2.5.

The analytical model shown in figure 2.4 is described by 21 coordinates. The angular positions of the gears, input and output inertias, and balance beam require nine coordinates. The axial positions of the pinion, first compound gear, second compound gear, and balance beam require four coordinates. The translations of the four gear shafts require another eight coordinates. Note that describing the translations of the four gear shafts with eight coordinates implies the assumption that the shafts do not tilt. This assumption was made because the shafts of the design are short compared with the gear diameters. By making this assumption, we avoid the need for another eight coordinates to describe the system. To further reduce the number of coordinates required, the moments of inertia of the helical pinion and the balance beam and the mass of the balance beam were considered negligible compared with the others in the system. Under these assumptions, the analytical model is described by a system of 18 equations of motion. The number of equations can be reduced to 17 by eliminating the rigid body mode of this semidefinite system.

For this system, the equations of motion were derived by the standard Lagrange method:

$$\frac{d\left[\left[\left(\frac{\partial L}{\partial \dot{q}_j}\right)\right]\right]}{dt} + \frac{\partial B}{\partial \dot{q}_j} - \frac{\partial L}{\partial q_j} = Q_j \qquad (j = 1,2,3,...,18)$$
(1)

where $L = T - V$, T is the total kinetic energy, V is the total potential energy, B is the energy dissipation function, q_j is the generalized coordinate, Q_j is the generalized force associated with each generalized coordinate q_j, and t is the time.

In applying the method, it was assumed that the gears contact along the theoretical line of action and that all stiffness elements were linear but, in the case of the gear meshes, were time-varying periodic functions. The damping elements were modeled with proportional damping expressed in terms of the damping ratio ζ, stiffness K, and inertia M, as $C = \sqrt{2\zeta KM}$. Damping in rolling element bearings was assumed negligible, and therefore the bearings were modeled with only stiffness elements. Each bearing was described with a 2-by-2 stiffness matrix to include cross-coupling effects at the bearings.

The kinetic energy of this system is formulated as

$$T = \frac{1}{2} \sum M_j \dot{q}_j^2 \qquad (j = 1,2,3,...,18)$$
(2)

The energy dissipation function of this system is formulated as

$$B = \frac{1}{2} \sum C_j \dot{q}_j^2 \qquad (j = 1,2,3,...,18)$$
(3)

The potential energy of this system was categorized as four groups. The first is the stored potential energy due to the distortion of the gear teeth. The equation describing this energy is most conveniently written by choosing a coordinate system with one coordinate parallel to the line of action. Therefore, to describe this stored energy, two coordinate systems were defined for each gear as shown in figure 2.5. The energy stored at a particular mesh is first expressed in the coordinate systems parallel to the line of action. Then, one of the two coordinate systems at each gear was chosen as the global system (i.e., the one in which the equations of motion were to be written). The second system was labeled as a local system. Reference frames with the asterisk super-script in figure 2.5 are local. The energy stored in the gear teeth was then described in only the global coordinates by transforming the local coordinates via rotational coordinate transformations. These coordinate transformations introduce the shaft locations of the gear train into the mathematical model as design/analysis parameters. For example, the potential energy stored in the helical mesh of the input pinon and second compound gear is expressed in the local coordinate system as

$$V_{2mh} = \frac{1}{2} K_{2mh}(t)\left[r_p \cos(\beta)\Psi_p - r_{2h} \cos(\beta)\Psi_{2h} + \cos(\beta)Y_p^* \right.$$
$$\left. - \cos(\beta)Y_2 + \sin(\beta)Z_p - \sin(\beta)Z_2 - e_{2h}(t)\right]^2 \tag{4}$$

To do the analysis, the local coordinate Y_p^* is transformed by

$$Y_p^* = Y_p \cos(\alpha_p) - X_p \sin(\alpha_p) \tag{5}$$

By applying relation (5) to equation (4), the potential energy can be expressed in only global coordinates as

$$V_{2mh} = \frac{1}{2} K_{2mh}(t)\left[r_p \cos(\beta)\Psi_p - r_{2h} \cos(\beta)\Psi_{2h} + \cos(\beta) \cos(\alpha_p)Y_p \right.$$
$$\left. - \cos(\beta) \sin(\alpha_p)X_p - \cos(\beta)Y_2 + \sin(\beta)Z_p - \sin(\beta)Z_2 - e_{2h}(t)\right]^2 \tag{6}$$

The potential energies stored in the other gear meshes were derived in a similar manner.

The second potential energy group is the energy stored in the bearings as a result of shaft translations, expressed as

$$V_b = \frac{1}{2} K_{xxb1}X_1^2 + \frac{1}{2} K_{yyb1}Y_1^2 + \frac{1}{2} K_{xxb2}X_2^2 + \frac{1}{2} K_{yyb2}Y_2^2$$
$$+ \frac{1}{2} K_{xxbp}X_p^2 + \frac{1}{2} K_{yybp}Y_p^2 + \frac{1}{2} K_{xxbB}X_B^2 + \frac{1}{2} K_{yybB}Y_B^2 \tag{7}$$

The third group is the potential energy stored in the twisted shafts, expressed as

$$V_s = \frac{1}{2} K_{s1}\left(\Psi_{1h} - \Psi_{1s}\right)^2 + \frac{1}{2} K_{s2}\left(\Psi_{2h} - \Psi_{2s}\right)^2$$
$$+ \frac{1}{2} K_{sp}\left(\Psi_i - \Psi_p\right)^2 + \frac{1}{2} K_{sB}\left(\Psi_B - \Psi_o\right)^2 \tag{8}$$

9

The fourth group is the potential energy due to the distortion of the balance beam support and the elements connecting the beam to the compound gear shafts, expressed as

$$V_a = \frac{1}{2} K_{z1}(Z_1 - L_{bal}\theta_{bal} - Z_{bal})^2 + \frac{1}{2} K_{z2}(Z_2 + L_{bal}\theta_{bal} - Z_{bal})^2 + \frac{1}{2} K_{bal}Z_{bal}^2 + \frac{1}{2} K_{zp}Z_p^2 \qquad (9)$$

By applying the Lagrange method, the system of 18 equations of motion was derived. This method was applied with the knowledge that the equations of motion would be solved numerically using a time-marching method. We assumed that the increment of time for the solution was small enough such that the time-varying mesh stiffness could be considered constant during a single time step. Of course, over a large time scale, the mesh stiffness is not constant. Therefore, after each solution step, the stiffness properties were reevaluated, and thus the time-varying mesh characteristics were included in the model. A typical equation of motion is presented in appendix A. The equations of motion were written with the displacement element terms $e_{ij}(t)$ appearing on the right-hand side of the equations as parts of the generalized forcing functions $Q_{ij}(t)$. In this study, the components of the friction forces that oppose axial motions were included whereas all other friction forces were assumed negligible. The generalized forcing functions were written so that sources of excitation such as gear hub-shaft runouts, gear geometry errors, and input-output torque fluctuations could be simulated. The time-varying mesh stiffness is a parametric excitation for the system that will cause vibrations even in the absence of generalized forcing functions.

The equations of motion were expressed in dimensionless forms using certain characteristic parameters inherent to the physical system. Appendix B includes a glossary of the dimensionless parameters and an explanation of how they were included in the model.

2.3   Solution Method

The dimensionless equations of motion were integrated in time by a fifth/sixth-order Runge-Kutta method (ref. 35). The solution step time size was selected to be no greater than 1/20 of the period of the helical gear mesh so that the gear mesh stiffness could be considered constant over that time frame. For this maximum step size, 16 167 solutions are required to simulate 1 revolution of the output gear. The solution of a system of equations of motion depends, of course, on the initial conditions and on the definition of the generalized forcing functions. The initial conditions (both positions and velocities) and forcing functions must be representative of the physical system so that a solution represents real physical phenomena.

For gear systems with only a single reduction stage, one may define the initial conditions of the system by an iterative method. Typically, it is assumed that the solution is periodic with the gear mesh period. An initial condition for the dynamic solution is assumed and is usually based on a static solution for a given load condition as a starting point. Then the equations are integrated for a time equal to the period of the gear mesh, and the final positions and velocities are compared with the initial conditions. Because the solution is assumed periodic, the initial and final conditions should be equal within some small tolerance. If they are not within tolerance, then a new set of initial conditions for the next iteration are calculated as a weighted average of the initial and final conditions of the previous iteration. This procedure is repeated until the proper initial conditions are found. Although this procedure was employed successfully, it has some limitations. One is that it does not directly allow inclusion of sources of vibration excitation except those whose frequency matches the gear mesh frequency. For example, to study the system response to accumulative pitch errors, the proper initial conditions for the case with no pitch errors is first found. Then it is reasoned that these initial conditions for the no-pitch-error case must be close to the case with pitch errors, and those conditions are used as the starting condition for the solution with pitch errors included. Another limitation is that this method cannot be applied to a multiple-

10

reduction-stage system in which there is more than one gear mesh frequency. Attempts to analyze a multiple-reduction-stage system were not successful (ref. 36).

To avoid these limitations, an alternate method of defining the initial conditions and forcing functions was devised. The present study begins the solution with the initial condition such that the system has no stored potential energy. This condition is met if all of the initial positions and velocities equal zero. Also, the net externally applied forces must equal zero. Conceptually, this can be thought of as the system operating under no load with all inertias rotating at a constant speed and with no vibrations. Of interest here are the motions of the system under design load. To make the transition from zero load to full load, input and output torques were applied as ramp functions, that is, as slowly and smoothly applied loads (shown in fig. 2.6). The torque applied to the output inertia was in the opposite direction of that applied to the input inertia and at every instant was equal in magnitude to the product of the input torque and the overall gear ratio. In this way, the net acceleration of the center of mass of the system was kept equal to zero. I have found that this method of starting the solution works well and avoids the limitations of the iterative procedure. The drawback is that a number of computations must be done to make the transition from no load to full load. Step functions (suddenly applied loads) were also tried to reduce the computations needed to make the transition from zero to full load, but the response of the system included very large vibrations not realistic for any physical system. All solutions in this study used the ramp loading function method.

Chapter 3

Analysis of Split Torque Gearbox Loads and Motion

3.0   Static Analysis

Although the actual dynamic loads of a gearbox are significantly different from the loads calculated by static analysis, the results of a static analysis can still reveal the characteristics of the gearbox and provide a baseline for a comparison with a dynamic analysis. For a static analysis of the NASA split torque gearbox design, the simplifying assumptions of no friction and laterally rigid shafts and shaft mounts were used. The bearing reactions calculated are given in table I. Note that, although the gearbox has symmetric geometry, the bearing reactions of the two compound shafts are not the same. Therefore, one can anticipate that the dynamic loads and motions of the two parallel paths will differ significantly. Also note that the sum of the bearing reactions of each compound shaft (locations 3 and 4 for one shaft, 5 and 6 for the other shaft) is on the order of 5000 to 7000 lb. On the other hand, the thrust loads generated by the helical gears will be on the order of 200 lb. The balance mechanism for load sharing operates on the principle that the balance beam will move and position the compound shafts in reaction to any difference in the thrust forces of the two parallel power paths. Considering the orders of magnitude of the bearing reactions and thrust forces, one can expect that the friction forces acting to prevent the axial motions of the compound shafts will be significant and should be included in the dynamic analysis.

TABLE I.—RESULTS OF STATIC ANALYSIS

[Bearing forces at full design load.]

Bearing location	Load		Load direction, deg
	kN	lbf	
1	3.57	800	24
2	4.57	1030	17
3	15.6	3520	137
4	6.05	1360	176
5	18.0	4040	174
6	14.3	3210	164
7	29.5	6640	335
8	16.2	3650	335

3.1   Modeling Bearing Stiffness

The work of R. Singh and T. Lim (ref. 37) was used to calculate the bearing stiffness characteristics used for the dynamic analysis. Their proposed bearing stiffness matrix in its most general form has 12 degrees of freedom. The number of degrees of freedom can be reduced by making assumptions about the shafts and mounts. Herein, to keep the total system model a reasonable size, I assumed rigid shafts and bearing mounts. Then, for the lateral directions, the bearing stiffness was described with a 2-by-2 matrix consisting of sub-components k_{xx}, k_{yy}, k_{xy}, and k_{yx} with the x-direction being parallel to the net force on the bearing. The numeric values for the bearing stiffness matrix components depend on the bearing geometry and load and on the material properties. Figure 3.1 shows the dependence of load on the stiffness coefficients k_{xx} and k_{yy} for the input pinion ball bearing (bearing number 1 of table I).

12

Once the bearing stiffness characteristics were calculated, two additional steps were taken to incorporate them in the system dynamic model. The first step was to account for the effect of the operating load on the bearing stiffness. One way to account for the load would be to calculate the bearing operating load at each time step of the dynamic solution, based on the initial conditions for that time step. However, to simplify the procedure and to save computing time, it was assumed that the dynamic bearing motions would be small compared with the mean bearing displacements. Therefore, the bearing stiffnesses were calculated for the static nominal load condition, and these values were used throughout the dynamic solution. Therefore, although the nonlinearities depicted in figure 3.1 were considered in calculating the bearing stiffness at the static load, the nonlinearities were not included in the equations of motion of this study. The ignored effect should be small as long as the bearing dynamic displacements about the mean displacement are small.

The second step to include the bearing stiffnesses into the system model was to account for the direction of the bearing loads. The global coordinate systems that were used to describe the lateral motions of the shafts were chosen to simplify the equations describing the stored potential energies due to distortions of the gear teeth (fig. 2.5 and eq. (4)). Also, the potential energies stored in the bearings (eq. (7)) were written using these same global coordinate systems. To calculate the coefficients of equation (7), the bearing stiffness matrices were determined for local coordinate systems parallel to the static bearing loads. Also, the angles between the static bearing loads and the global coordinate systems were determined. The bearing stiffness matrices were then transformed to the global coordinate systems by

$$[K] = [A]^T[K^*][A]$$

(10)

where

[K]   matrix in global coordinate system

$[A]^T$ transpose of [A]

$[K^*]$ matrix in local coordinate system

[A]   rotational coordinate transformation matrix

The results of the calculations for one bearing are shown in table II.

TABLE II.—BULL GEAR ROLLER
BEARING STIFFNESS MATRIX

Coordinate system	Stiffness, $K_b = \begin{bmatrix} k_{xx} & k_{xy} \\ k_{yx} & k_{yy} \end{bmatrix}$, 10^6 lb/in.
Local	$\begin{bmatrix} 11.4 & 6.9 \\ 6.9 & 9.5 \end{bmatrix}$
Global	$\begin{bmatrix} 16.4 & -3.7 \\ -3.7 & 4.6 \end{bmatrix}$

13

3.2 Modeling Gear Stiffness and Damping

A spring, a damper, and a displacement element are included in the mathematical model to simulate each gear mesh. The analytical code was written assuming that the spring stiffness and displacement elements were constant over each time step of the numeric solution but varied over larger time scales. Therefore, the gear mesh stiffness and damping were calculated at the beginning of each time step. In this study, the gear mesh stiffness and damping were assumed to be periodic functions of time with a fundamental period equal to that of the mesh period for a constant pinion speed. Following is a description of the methods and assumptions used to define these functions to model the particular configuration and design of this study.

For this study, I have assumed that the gear mesh provides only a small amount of damping. A damping ratio ζ of 0.01 was used for the proportional dampers to simulate a lightly damped system.

The time-varying characteristics of the spur gear mesh stiffness were defined by first using the work of Cornell (ref. 26) to determine the compliance of a single pair of contacting gear teeth. Cornell defined the compliance along the line of action in terms of gear dimensions and material properties. The method includes tooth bending effects, fillet and foundation effects, and deformation at the hertzian contact. Rim effects, which in some cases can be significant (refs. 27 and 38), were not considered in this study because the design has fairly thick rims and calculating individual tooth loads was not a part of this study. The geometric preprocessor of the gear dynamics computer program GEARDYNMULT (refs. 30 and 31) was used to calculate a set of coefficients via Cornell's method. These coefficients define the tooth pair compliance of a single pair of contacting teeth as a function of the position along the line of action. To calculate the gear mesh stiffness for a particular angular position of the pinion, the position of contact along the line of action for each tooth pair in contact was calculated. The tooth pair stiffness was then calculated using the information from the output of the GEARDYNMULT code, and the tooth pair stiffnesses for all pairs of teeth in contact were summed to calculate the total gear mesh stiffness. This procedure was repeated for a number of angular positions to adequately determine the periodic gear mesh stiffness. Details of the calculation method and the GEARDYNMULT computer program output are given in appendix C. The single tooth pair compliance as a function of contact position along the line of action is shown in figure 3.2. The mesh stiffness, including the effect of the changing number of teeth in contact, is shown as a function of pinion position in figure 3.3. Note that the maximum stiffness is almost twice the minimum stiffness. The mesh stiffness shown in this figure can be defined as a function of time by assuming a constant pinion speed. A piecewise smooth function was fit to the mesh stiffness data to create a time-varying mesh stiffness function for the split torque dynamics code.

The procedure just described was extended to define the time-varying characteristic of the helical mesh. The method of Cornell applies directly only to spur gears. Therefore, to extend the method, the helical gears were modeled as a number of staggered spur gears as illustrated in figure 3.4. This approximation accounts for the stiffness effects in the transverse plane and accounts for the moving contact position along the length of the helical tooth. The axial stiffness effects are not accounted for with this approximation. However, because the helix angle of this design is small (6°), this ignored effect should be small. The helical gear dimensions in the normal plane were used as input to the computer program GEARDYNMULT to determine Cornell's compliance coefficients of each spur gear slice. The face width of each slice equaled the axial face width of the gear divided by the number of staggered spur gears. For a given angular position of the helical pinion, the number of staggered spur gear elements with teeth in contact and the contact position along the lines of action were calculated. The stiffnesses for all spur gear pairs in contact were summed to calculate the gear mesh stiffness for that position of the pinion and then were repeated for several different angular positions. The computer code used for the calculations and the output are given in appendix D. The results of the calculations for two different cases are shown in figure 3.5; (a) a coarse model with 24 spur gear slices and (b) a fine model with 240 spur gear slices. It is interesting to note that, although the stiffness variation for spur gears is nearly 2 to 1, the stiffness for the helical gears varies by only 14 percent. The function shown in figure 3.5(b) was redefined as a function of time

by assuming a constant speed for the pinion. A piecewise smooth function was fit to the mesh stiffness data to create a time-varying mesh stiffness function for the analytical code.

A unique property of gearboxes that have multiple load paths, such as split torque and planetary designs, is the phase relationships of the gear meshes. Consider a pinion driving two gears. If the length of the arc along the pitch circle joining the two pitch points (fig. 3.6) is an integer multiple of the circular pitch, then both meshes will pass through the pitch point at the same instant of time, and the mesh properties can be considered in phase. For the design studied here, the mesh properties are out of phase as shown in figure 3.7. Although for a given set of gears and shaft locations the mesh phase relationships are defined, the phase relationships were included as a variable in the analytical model so that the effect of mesh phasing could be assessed independently. The mesh phasing can be considered a design variable.

3.3 Modeling Manufacturing Errors

To simulate the dynamics of a real system, the loaded static transmission error of the analytical model should match that of the physical system. Because the stiffness elements were defined as flexible gear teeth with assumed perfect involute shapes under load (i.e., with proper profiles for the full load condition), the displacement elements of the gear mesh model were defined to simulate the main component of the unloaded static transmission error attributable to manufacturing errors. The actual errors of the gears were not known or measured, but the manufacturing specifications were AGMA class 12 quality. Based on typical single-flank and index variation measurements, illustrated in figure 3.8, the total transmission variation often has a large component periodic with the gear revolution. This component of the total transmission variation is mainly a combination of accumulated pitch error and gear runout. In this study, the displacement element of the gear mesh was defined as the sum of two sinusoidal functions, one function for each gear in mesh, with the period of each sinusoidal function equal to the period of gear revolution. The amplitude of the sinusoidal functions can be varied to simulate different levels of gear quality. The simulated unloaded and loaded static transmission error for rigid bearings, full design torque, and one set of assumed error amplitudes for one of the gear meshes are shown in figure 3.9.

Assembly error, a manufacturing error unique to split torque arrangements, was included in the model. A split torque arrangement creates a locked loop of gearing as illustrated by the heavy line of figure 3.10. Under a nominal light load, each of the four gear meshes in the loop will be engaged if, and only if, the splitting mesh gear and combining mesh pinion carried on each common shaft have been assembled with the required relative angular relationship. This condition can also be thought of as the two gears requiring a particular tooth timing relationship. One can anticipate that because of manufacturing limitations, any real gearbox will not have the required relationship but will have some error in the assembly. Under light load, this error will cause a gap at one of the four gear mesh locations. The purpose of the various proposed split torque load-sharing methods is to compensate for or minimize the effect of this gap. In this study, the assembly error was simulated by adding a mean value to one gear's sinusoidal error function described in the preceding paragraph. Therefore, referencing equation (4), the potential energy stored in the gear mesh was adjusted to account for the gap that exists under no load by adding a constant term to the sinusoidal function $e_{2h}(t)$ that defines the displacement element. The numeric value of the constant term can be adjusted to simulate varying amounts of assembly error.

3.4 Modeling Friction

Although the friction forces from tooth sliding were neglected, the friction forces that tend to oppose the axial motions of the helical gears in response to the thrust of the meshing helical teeth were included in the model. Friction is present both at the contacting gear teeth and at the bearing supports. This friction opposes

axial motions of the gears. The magnitude of the friction forces can be significant compared with the thrust forces, especially if the helix angle of the mesh is small. Therefore, the friction effects were included in the analytical model. The friction force was calculated at the beginning of each time step and was assumed constant over the small time steps of the solution. The following procedure was used to calculate the magnitude and direction of the friction forces. First, for each shaft carrying a helical gear, the maximum possible total friction force was calculated as

$$F_{max} = F_b\mu_b + F_m\mu_m \tag{11}$$

where

F_b sum of magnitudes of bearing forces on shafts

μ_b coefficient of friction at bearings

F_m sum of magnitudes of tooth mesh contact forces

μ_m coefficient of friction at meshing gear teeth

Second, two separate cases must be considered, one for the shaft at rest and one for the shaft in motion. The shaft was considered at rest if the magnitude of the velocity was less than 0.00025 in./sec (the shaft velocity was compared with this small value rather than with 0 to account for truncation and roundoff errors of the numeric solution).

For the shaft in motion, the friction force opposes the motion and so was calculated as

$$F_{frict} = [sign] \cdot F_{max} \tag{12}$$

where the [sign] is −1 if velocity > 0 or is +1 if velocity < 0. For the shaft at rest, the friction force is in the direction opposite the net of all other forces and has a magnitude equal to the lesser of the net of the other forces and the maximum possible friction force. So, for the shaft at rest, the net of the other forces was calculated using the matrix form of the equation of motion:

$$F^* = -\{[K]\{Y\} + [C]\{\dot{Y}\}\} + F_e \tag{13}$$

where

[K]   relevant row of stiffness matrix

{Y}   generalized displacement vector

[C]   relevant row of damping matrix

{Ẏ}   generalized velocity vector

F_e relevant term of generalized force vector

Then, the friction force was calculated as

$$F_{frict} = [sign] \cdot \text{Minimum of} \begin{cases} |F^*| \\ F_{max} \end{cases} \tag{14}$$

where the [sign] is −1 if $F^* > 0$ or is +1 if $F^* \leq 0$.

The friction force calculated using the procedure just described was added as a constant to the generalized force vector {F}, and then the equations of motion were integrated. The magnitude and direction of the friction forces were recalculated at the beginning of each step of the time-marching solution.

3.5 Modeling A Closed-Loop Test Stand for Open-Loop Analysis

Although the analytical model of this study is an open-loop system, the experimental rig that was used to test the gearbox design is part of a closed-loop system (fig. 3.11). Here, the terms "open loop" and "closed loop" are not used in the sense of control theory but as a description of the power flow in the system. The closed-loop system consists of nominally identical test and slave gearboxes loaded against each other. The drive motor rotates the system at the desired speed. This closed-loop system is often used for testing gear systems because it can be done at high power by establishing a large torque in the loop while the drive motor needs only to supply a relatively small amount of power to overcome frictional losses. If the gearbox were tested in an open-loop facility, a larger drive motor and a large power-absorbing unit would be required. Although the closed-loop system is convenient and economical for experiments, analytical codes are written to analyze the open-loop structure of field designs. Since it is desirable to compare the analytical results of this study to experimental data as it becomes available, a method for modeling the closed-loop configuration of the experimental facility was developed.

One option for analyzing the motions of the experimental test rig was to expand the analytical model to include the inertias and stiffnesses of the slave gearbox and drive motor. This mathematical model would have many more equations and require much effort to develop. A second option, used for this study, was to model the closed-loop system with an open-loop model (fig. 3.12) and select numeric values for the input and output inertias and stiffnesses of the open-loop model to best simulate the closed-loop system. I propose that one apply these two rules to determine the numeric values:

(1) The kinetic energy of the input and output inertias of the analytical model should equal the kinetic energy of all the physical system components that are not directly represented in the analytical model.

(2) The ratio of the input inertia to the output inertia of the analytical model should equal the ratio of the stiffnesses of the two branches of the parallel paths to the drive motor.

The first rule matches the total kinetic energies of the analytical and the physical systems; the second rule matches the exchange of potential and kinetic energies in the two systems. For the physical system, vibration in the test gearbox tends to cause motion of the drive motor through both of the two parallel paths of the closed-loop system. If one ignores inertial effects for the moment, the torque induced in each path by vibration is proportional to the stiffnesses of that path. The larger portion of inertia is assigned to the stiffer path to match the way potential energies are stored and imparted to the drive motor. Also, by applying the second rule, the natural frequency of the output inertia/stiffness pair will match that of the output inertia/stiffness pair. Therefore, in the analytical model the frequency responses of the input and output inertias to some excitation within the test gearbox tend to be the same. This matched response is similar to the physical closed-loop system where there is only one "group" of inertias and stiffnesses responding to the excitation.

For the test rig I studied, all the components in the loop have approximately the same stiffness relative to the load carried; one exception was the torquemeter located between the two bull gear shafts (fig. 3.11). To achieve good sensitivity, the torquemeter has a stiffness that is approximately 1 order of magnitude less than that of the other components, which were designed for strength using conservative methods. As a result, approximately 90 percent of the total inertia of the drive motor and slave gearbox was assigned to the input inertia, and approximately 10 percent was assigned to the output inertia. Details of the calculations to determine the numeric values are given in appendix E.

17

3.6 Dynamic Analyses and Results

Dynamic analyses were completed for five cases representing different sets of operating conditions or assumptions. Following is a description of the simulated conditions and the results for each case.

3.6.0 Case 1—Nominal analysis

The first case investigated, herein termed the nominal conditions, used some simplifying assumptions so that some experience with the computer code could be gained and a baseline could be established for further studies. The following simplifying assumptions were used for case 1: no assembly error was present; Coulomb friction forces in the directions parallel to the shaft axes were zero; and the amplitudes of the total accumulative pitch variations of the gears were small, on the order of 0.00005 in. An analysis was conducted over the range of dimensionless time (0 to 2300) wherein the relation between dimensionless time and dimensioned time was

$$T = \omega_p t \tag{15}$$

where

T   time, dimensionless

ω_p speed of input pinion, 919.23 rad/sec

t   time, sec

Therefore, the 2300-dimensionless time analyzed represents about 2.5 sec of operation with the gearbox running at full rated speed. The total simulation includes 14.5 revolutions of the low-speed output shaft. The system was loaded to full rated torque using ramp-shaped forcing functions that increased the load linearly from zero load at time T = 0 to full load at time T = 500. The complete input data set for the computer code is given in table III.

The simulated dynamic shaft torques are shown and compared with the shaft torques for ideal load sharing under static conditions in figure 3.13. The dynamic shaft torques vary about the expected static solution. The torques of the two compound shafts, plotted together in figure 3.13(b), show nominally good load sharing but with significant dynamic peaks.

The simulated lateral shaft vibrations, plotted as shaft orbits for time T = 900 to 2300, for all four shafts are shown in figure 3.14. All the bearing orbits are stable and have reasonable amplitudes. It is interesting that the orbits of the two compound shafts are significantly smaller than either the input shaft or output shaft orbits.

The simulated axial motions of the input shaft and compound shafts are shown in figure 3.15 (the output shaft carries only a spur gear and was assumed fixed axially). In the absence of friction, as assumed herein, large axial motions occur. Note that the phase difference in the sinusoidal plots of the two compound shafts indicates a rocking motion of the balance beam as it functions to balance the torque split.

18

TABLE III.–COMPUTER ANALYSIS INPUT FILE

Value for computer code	Description		Units
9.1923D+02	Speed, input pinion		rad/sec
6.0000D+00 122.50D+00 138.72D+00 48.620D+00 50.200D+00	Helix angle, input pinion Pinion shaft angle Number 1 Number 2 Bull gear shaft angle		deg
2.5000D+06 2.0500D+05	Stiffness, beam center support Stiffness, beam to gear shaft		lb/in.
0.0000D+00 35.000D+00 140.00D+00 290.00D+00 70.000D+00 340.00D+00	Displacement function phase angles	Helical pinion Helical gear 1 Helical gear 2 Spur pinion 1 Spur pinion 2 Bull gear	deg
-38.400D+00 163.50D+00	Mesh phase angles	Helical mesh Spur mesh	deg
1.0000D-05 1.5000D-05 6.0000D-05 9.0000D-05	Displacement function amplitudes components	Helical pinion Helical gear Spur pinion Bull gear	in.
13.000D+06 1.2000D+05 9.0000D+06	Shaft torsional stiffness	Compound Input Output	in.-lb/rad
3.6590D+00 1.2235D+00 0.94425+00 7.9754D+00	Base radii	Helical gear Spur gear Helical pinion Bull gear	in.
4.5000D+00 10.240D+00 65.000D+00	Mass	Input pinion shaft Compound shafts Bull gear shaft	lb
46.800D+00 23.000D+00 12.000D+00 1030.0D+00 3510.0D+00	Inertias	Input Helical gear Spur pinion Bull gear Output	lb-in.^{2}
000.00D+00 1.0000D+05 1.0000D-02	Start time Number of solution steps Step size		Dimensionless time
0.0000D-00	Assembly error		in.
0.0200D+00 0.0050D+00	Coefficient of friction	Gear teeth Bearings	Dimensionless

The results shown in figures 3.13 to 3.15 indicate that the computer solutions are mathematically robust. The ramp-shaped forcing function method for establishing the initial conditions produces a periodic solution. A method for achieving dynamic solutions of split torque gearbox designs was demonstrated.

3.6.1 Case 2—Effect of Assembly Error in Presence of Friction

The effect of assembly errors and friction on the performance of the split torque design was studied by completing a dynamic analysis. The analysis of case 1 was repeated except that friction forces parallel to the shaft axes and assembly error were added. Here, it was assumed that under light load a gap was present between the helical pinion and the helical gear of the first compound shaft. Four different simulations, using assembly error magnitudes of 0.0000, 0.0013, 0.0026, and 0.0040 in., were completed. The 0.0040-in. magnitude of assembly error represents the maximum that can exist and still permit assembly of the gearbox. That is, with the 0.0040-in. assembly error at the helical gear mesh, the back side of the pinion tooth just touches a tooth on the gear. The friction coefficients assigned were 0.005 for the bearing supports and 0.020 for the contacting gear teeth. These values were assumed based on data reported by other researchers (refs. 39 and 40). Solutions were completed to cover 0- to 2400-dimensionless time assuming the gearbox running at full rated speed and using the same ramp shaped loading function as used for case 1.

The predicted axial motions for the solution with friction present but no assembly errors are shown in figure 3.16. The axial motions were greatly reduced compared with those for the solution with no friction (fig. 3.15). Once the steady-state positions are reached, there exists only a small axial motion of the input shaft while the two compound shafts are essentially at rest. The steady-state displacement of the two compound shafts is not equal, indicating that the balance beam has rotated. The balance beam motions both with and without friction present and with zero assembly error are shown in figure 3.17. Without friction, there is a large, low-frequency oscillation of the balance beam. However, with friction included in the analysis, the beam rotates toward a steady-state position without vibration. These results show that it is important to include friction in the model to predict the performance of this design.

The influence of assembly errors and friction on the shaft torques is significant. The predicted shaft torques for the solution assuming an 0.0040-in. assembly error and with friction present are shown in figure 3.18. The input and output shaft torques vary about the static solution and are essentially identical to the solution with no friction and no assembly error (fig. 3.13). However, because of the assembly error, the compound shafts no longer carry the same mean torque. Also, note that the frequency content of the dynamic torques of the two compound shafts is different. This difference in frequency content is more difficult to see but is also present in the data of figure 3.13. It is not surprising that the two compound shaft torques differ because the loading of the two shafts is not the same, as was determined even by a simple static analysis (table II). The differences between these two shafts were studied further and are discussed in section 3.6.4.

The influence of the assembly errors on load sharing was studied. The motion of the balance beam for four different magnitudes of assembly error is shown in figure 3.19. The beam rotates toward a position to balance the load sharing, but because of friction, the balancing is not exact. The significance of this phenomenon is shown in figure 3.20 where the mean torque ratio is defined as the mean torques of the compound shafts normalized to the total mean torque. For the ideal case in which each shaft carries one-half of the total power, the mean torque ratio for each shaft would equal 50 percent. The relation between the assembly error and the mean torque ratio is linear. The maximum mean shaft torque for the conditions assumed here is approximately 55 percent of the total whereas the ideal condition is 50 percent. Figure 3.20 suggests that an assembly error of about 0.0002 in. is an optimal tooth indexing relationship because the total compliance of the two load paths, including the coupling of lateral and rotational displacements, influences the amount of torque carried in each of the parallel paths. The complete system stiffness represented by the stiffness matrix used in this analysis must be considered to precisely determine the optimal tooth indexing positions.

3.6.2 Case 3—Effect of Friction Magnitude

Seven dynamic analyses were completed to study the effect of the friction coefficient on the effectiveness of the balance beam concept. Seven analyses were completed. For each, the coefficient of friction at the bearings and at meshing gear teeth was assumed to be equal. The coefficient of friction for the seven analyses was varied from 0.001 to 0.050. An assembly error of 0.0040 in. at one helical mesh was used for each analysis. The remainder of the input variables for the computer code matched those of case 1 (given in table III). The ramp loading method was used, with the load increasing linearly from 0 at dimensionless time 0 to full load at dimensionless time 500. The calculations were completed to include the dimensionless time 0 to 1600.

The steady-state portion of the solutions, from dimensionless time 700 to 1600, was used to calculate the mean torque ratios for each analysis. The mean torque ratios are a measure of the effectiveness of the balance beam mechanism in balancing the power split. These ratios are plotted as a function of the friction coefficient in figure 3.21. For a friction coefficient greater than about 0.003, the balance beam is for practical purposes locked in place by the friction forces. The mean torque ratios of 45 and 55 percent indicate the balance beam is not an effective device for load sharing unless the friction coefficient is less than 0.003. In practice, the coefficients are likely to be in the range 0.005 to 0.020 (refs. 39 and 40). It may be necessary to increase the helix angle of the helical gears (from the very shallow 6° of the design studied in this report) to improve the load sharing of the balance beam split torque transmission. Changing the helix angle will affect the entire transmission design, including the load capacity. This is beyond the scope of this paper.

3.6.3 Case 4—Effect of Bearing and Tooth Stiffnesses

Calculations for four analyses were completed to study the relative contributions of bearing and tooth stiffnesses to the torque-sharing characteristics of the design. For all calculations, the friction coefficients used were 0.020 at the gear teeth and 0.005 at the bearings. Also, an assembly error of 0.0040 in, for the helical mesh of the first compound shaft was used for all cases. First were two static analyses, one assuming both the gear teeth and bearings were rigid and a second assuming that the gear teeth were flexible but the bearings rigid. For these two analyses, it was assumed that the balance beam did not rotate. The third was a dynamic analysis that assumed normal gear tooth stiffnesses and very stiff bearings. The values used for the bearing stiffnesses in this analysis method were 500 times greater than those calculated for the actual design. The fourth was a dynamic analysis assuming flexible gear tooth and bearing stiffnesses.

The mean torque ratios were calculated for each of the four analyses just described. The resulting torque ratios are given in table IV. In analysis 1, both bearings and gear teeth assumed rigid with an 0.0040-in. assembly error, the code predicts that compound shaft 1 carries all the torque whereas compound shaft 2 rotates but transmits no load. This first analysis assumes that only the compound shaft torsional deformation contributes to accommodating the assembly error. This analysis is overly conservative in establishing a required tolerance for the assembly error.

The second analysis includes the gear tooth flexibility in the calculations. Comparing the results of analyses 1 and 2 as presented in table IV, one can infer that the gear tooth deformation does significantly contribute to accommodating the assembly error. Analysis 2 predicts that the torque will split 90 to 10 percent between the two load paths in the presence of an 0.0040-in. assembly error. This second analysis is also overly conservative in establishing an assembly error tolerance.

The third analysis is dynamic. Gear teeth were assumed flexible and the bearings very stiff. The predicted mean torque ratios using the dynamic analysis are quite different from those of the two static analyses. The improved load sharing predicted by this dynamic analysis compared with that predicted by the static analysis is

a combined result of adding some flexibility at the bearings and of including the effect of balance beam motion in the model.

The fourth analysis is similar to the third except that the bearings were assumed flexible. Comparing the mean torque ratios calculated by analyses 3 and 4 as presented in table IV, one can infer that the bearing deformations contribute significantly to accommodating the assembly error. The results of this study indicate that gear tooth and bearing flexibility significantly affect the torque-sharing property of this design. Along with shaft torsional flexibility, both should be included in the calculation for establishing a desired assembly error tolerance for a given design. This dynamic analysis could be used to predict the mean torque ratio for a given assembly error.

TABLE IV.—COMPARISON OF ANALYSIS METHODS

FOR PREDICTING TORQUE RATIOS

Analysis	Shaft	
	1	2
	Torque ratio[a] = $100 \times \dfrac{\text{Mean shaft torque}}{\text{Total mean torque}}$, percent	
1. Static analysis (rigid bearings and gear teeth)	100.0	0
2. Static analysis (rigid bearings, flexible gear teeth)	90.8	9.2
3. Dynamic analysis (very stiff bearings, flexible gear teeth)	71.6	28.4
4. Dynamic analysis (flexible bearings and gear teeth)	56.1	43.9

[a]Assembly error, 0.0040 in.

A comparison of some of the results of analyses 3 and 4 reveals some coupling of the lateral and torsional vibrations of the system. For example, when the shaft torques for the case with very stiff bearings (fig. 3.22) are compared with those for the case with flexible bearings (fig. 3.18), there exists a high-frequency component in the dynamic torques of the compound shafts for the case with stiff bearings. This indicates that, depending on the bearing stiffnesses, the lateral and torsional vibrations could be strongly coupled in this system. Also, figures 3.18 and 3.22 illustrate the contribution of bearing flexibility to improving the load sharing of this design.

The contribution of bearing flexibility to accommodating assembly error is further illustrated by the results of analysis 4 as presented in figures 3.23 and 3.24 in which the dynamic gear mesh deformations are plotted. These deformations can be considered the sum of several components (described by eq. (4)) that are also plotted in the figures. Note that, although the assembly error (represented by the mean of the gear error component) and the angular motions tend to cause compression of the gear mesh spring element, the lateral motion cancels the compression by a significant amount. It is also interesting to note that the low-frequency part of the angular

vibration tends to be transmitted to the lateral vibration; on the other hand, the high-frequency part of the angular vibration is not transmitted to the lateral vibration.

3.6.4 Case 5—Effect of Total Composite Gear Error

The effect of total composite gear error on the dynamics of the system was investigated. The main component of a typical composite gear error due to manufacturing inaccuracies was modeled in this study by defining the displacement elements as a sinusoid function whose frequency was equal to that of the mean gear rotation speed (i.e., shaft frequency). This simulates both runout and typical accumulated pitch error. The amplitudes of the sinusoid functions for the dynamic analyses of both a small error (case 1, section 3.6.0) and a large error (case 5) are listed in table V. Dynamic analyses were completed for the range of dimensionless time 0 to 1600.

TABLE V.—MAGNITUDE OF DISPLACEMENT

ELEMENT FUNCTIONS FOR LARGE

AND SMALL GEAR ERRORS

Gear element	Case	
	Small error	Large error
	Displacement element amplitude, in.	
Helical pinion	1.0×10^{-5}	12.0×10^{-5}
Helical gears	1.5	15.0
Spur pinions	6.0	14.0
Spur gears	9.0	20.0

The effect of gear error on the system dynamics is significant. The dynamic torque for the compound shafts is much greater for the large gear error case (fig. 3.25) than for the small gear error case (fig. 3.18).

To further investigate the phenomenon, the shaft torque data were transformed to the frequency domain using the Fast Fourier Transform techniques. The mean torques were removed from the torque data before the transforms were done. The power spectral densities of the input and compound shaft torques between 0 and 10 000 Hz are shown in figure 3.26. The main components of the input shaft torque are the shaft frequencies, caused by the gear error excitation, and the helical mesh fundamental frequency. There are also sidebands about the helical mesh fundamental spaced at shaft frequencies, which is common in gearbox vibration spectra. The main components of the compound shaft torque are the shaft frequencies and the spur mesh frequency with its harmonics. On first inspection, the frequency spectra of the two compound shafts may seem very similar although the time domain representations look very different. However, on closer inspection, differences are also evident in the frequency domain. Figure 3.27 shows the power spectral densities between 0 and 200 Hz. Note that, even though both shafts are excited by the same sources, compound shaft 2 has a much greater response at its rotation frequency. This response may be attributed to the differences in the mean bearing loads, which change the bearing stiffnesses. Figure 3.28 shows the power spectral densities between 800 and 1200 Hz. The sidebands about the spur mesh fundamental are spaced at the compound shaft frequency and are much greater for shaft 2 than for shaft 1. Again, this comparison illustrates that, although the gearbox has a symmetric geometry, the dynamics of the two power paths are not the same.

To further investigate the effect of a large gear error on the system, the shaft orbits, gear mesh forces, and dynamic transmission errors were calculated. A comparison of figure 3.29, showing the shaft orbits for large

gear errors, with figure 3.14, showing shaft orbits for small gear errors, reveals that the input shaft orbit has grown substantially whereas the compound and output shaft orbits are relatively similar. There seems to be some weak coupling between the lateral and torsional vibrations at the shaft frequencies.

The helical gear mesh forces are shown in figures 3.30 and 3.31. The variation of the helical mesh force over one mesh period (figs. 3.30(a) and 3.31(a)) is about 100 lb for both load paths, and the shapes of the plots over one mesh period are very similar. On the other hand, comparing figures 3.30(b) and 3.31(b) reveals a large variation in the gear mesh force at the input shaft frequency for helical mesh 1 that is not present for helical mesh 2.

The spur mesh forces are shown in figures 3.32 and 3.33. The variation of the spur mesh force over one mesh period (figs. 3.32(a) and 3.33(a)) is about 5000 lb for mesh 1 and 3500 lb for mesh 2. Also, the shapes of the waveforms over one mesh period are different, which may be caused by the difference in the mesh phasing illustrated in figure 3.7. The variations in spur mesh forces over shaft frequencies (figs. 3.32(b) and 3.33(b)) are very similar for the two load paths.

The predicted dynamic transmission errors were calculated for each pinion/gear pair by subtracting the ideal gear angular position from the position predicted by dynamic analysis. The predicted transmission errors are shown in figures 3.34 and 3.35. A positive number indicates that the angular position lags the position of the ideal gear. As with the torque and gear mesh forces, there is a significant low-frequency component due to the total composite gear error of the spur gear. The dynamic transmission errors of the two helical gears (fig. 3.34) are very similar. For the spur gears, however, the transmission error of the first gear includes a component at the input shaft frequency (fig. 3.35(a)) that does not appear in the transmission error of the second gear (fig. 3.35(b)).

The results of the analyses just presented show that the frequency responses of the two power paths are different even though they have the same geometry. The phenomenon of sidebands spaced at shaft frequencies about gear mesh fundamental frequencies (as often seen in gearbox vibration spectra) was simulated by modeling the gear errors as sinusoid functions. A method for simulating the effect of accumulated pitch errors and/or runout errors on the performance of a gearbox has been presented and demonstrated, but a correlation between manufacturing accuracy and gearbox performance was not attempted. The magnitude of the composite gear error excitation used in this example is likely to be larger than that which actually occurs in practice, especially for the helical mesh. When compared with spur gears, the larger overall contact ratio of helical gears tends to better smooth out the effects of index variation. It is not possible to investigate this concept with the model used here because the individual tooth index errors are not modeled. Instead, the net effect is approximated by a single time-varying displacement element. A possible area of future work would be to refine the method for directly modeling gear index errors.

Chapter 4

Summary of Results

A dynamic analysis method for split torque transmissions was presented and applied to study the load sharing and other characteristics of a split torque design. A mathematical model was developed by applying the Lagrange method to derive a system of 18 equations of motion to describe the design. The effects of time-varying mesh stiffness, friction, and manufacturing errors were included in the model. The equations of motion were made nondimensional and were solved using a fifth/sixth-order Runge-Kutta method. Several studies were completed to evaluate the design.

The following specific methods were developed and applied

(1) A method for calculating a time-varying mesh stiffness for helical gears was developed by extending Cornell's method for spur gears. The helical gears were modeled as a set of staggered spur gears.

(2) A ramp loading method was developed and used to define the initial conditions of the set of equations of motion.

(3) A method for analyzing a closed-loop system by using an open-loop model was developed and applied.

(4) The effects of runout and accumulated pitch errors were simulated by defining the displacement element of the gear mesh model to be the sum of two sinusoid functions whose periods equal those of the gear rotation periods.

(5) A mathematically robust method for the dynamic analysis of split torque transmissions was developed and demonstrated.

The following results were obtained:

1. Even though the gearbox geometry is symmetric, the loads and motions of the two power paths differ.

2. Friction must be included in the model to properly evaluate the balance beam mechanism and the performance of the design.

3. For the design studied, the balance beam mechanism is not an effective device for load sharing unless the coefficient of friction is less than 0.003.

4. The relation between the magnitude of assembly error and the resulting mean torque ratios of the two power paths is linear.

5. The complete system stiffness as represented by the stiffness matrix used in this analysis must be considered to precisely determine the optimal tooth indexing positions.

6. For the design studied, both gear tooth and bearing flexibility should be considered along with shaft torsional flexibility for establishing a required tolerance for assembly errors.

7. The phenomenon of sidebands spaced at shaft frequencies about gear mesh fundamental frequencies, as often occurs in real gearbox vibration spectra, was simulated by modeling the main component of typical total composite errors as sinusoid functions.

Appendix A

Typical Equations of Motion for the Split Torque Transmission

The system has 18 equations of motion. The equation of lateral displacement of the first compound gear Y_1 is presented below:

$$M_1\ddot{Y}_1 + \{\cos^2(\beta)K_{1mh} + \cos^2(\alpha_1)K_{1ms}$$

$$+ [r_p \cos^2(\beta)K_{1mh}]^2/[r_p^2 \cos^2(\beta)(K_{1mh} + K_{2mh}) + K_{sp}] + K_{yyb1}\}Y_1 - \{\sin(\alpha_1)\cos(\alpha_1)\ K_{1ms}\}X_1$$

$$- \{[(r_p \cos^2(\beta)K_{1mh})(r_p \cos^2(\beta)\sin(\alpha_p)K_{2mh}]/[r_p^2 \cos^2(\beta)(K_{1mh} + K_{2mh}) + K_{sp}]\}\ X_p - \{\cos^2(\beta)K_{1mh}$$

$$- ([r_p \cos^2(\beta)K_{1mh}]\{r_p \cos^2(\beta)[K_{1mh} + \cos(\alpha_p)K_{2mh}])/[r_p^2 \cos^2(\beta)(K_{1mh} + K_{2mh}) + K_{sp}]\}Y_p$$

$$- \{[(r_p \cos^2(\beta)K_{1mh})(r_p \cos^2(\beta)K_{2mh}]/[r_p^2 \cos^2(\beta)(K_{1mh} + K_{2mh})] + K_{sp}\}Y_2 - \{\cos(\alpha_1)K_{1ms}\}Y_B$$

$$+ \{\cos(\beta)\sin(\beta)K_{1mh} + [(r_p \cos^2(\beta)K_{1mh})(r_p \cos(\beta)\sin(\beta)K_{1mh})]/[r_p^2 \cos^2(\beta)(K_{1mh} + K_{2mh}) + K_{sp}]\}Z_1$$

$$- \{[(r_p \cos(\beta)\sin(\beta)K_{2mh})(r_p \cos^2(\beta)K_{2mh})]/[r_p^2 \cos^2(\beta)(K_{1mh} + K_{2mh}) + K_{sp}]\}Z_2 - \{\cos(\beta)\sin(\beta)K_{1mh}$$

$$+ [(r_p \cos^2(\beta)K_{1mh})(r_p \cos(\beta)\sin(\beta)(K_{1mh} + K_{2mh})]/[r_p^2 \cos^2(\beta)(K_{1mh} + K_{2mh}) + K_{sp}]\}Z_p$$

$$- \{[(K_{sp})r_p \cos^2(\beta)K_{2mh}]/[r_p^2 \cos^2(\beta)(K_{1mh} + K_{2mh}) + K_{sp}]\}\ \Psi_i$$

$$+ \{r_{1h} \cos^2(\beta)K_{1mh} + [(r_p \cos^2(\beta)K_{1mh})(r_pr_{1h} \cos^2(\beta)K_{1mh})]/[r_p^2 \cos^2(\beta)(K_{1mh} + K_{2mh}) + K_{sp}]\}\Psi_{1h}$$

$$+ \{[(r_p \cos^2(\beta)K_{1mh})(r_pr_{2h} \cos^2(\beta)K_{2mh})]/[r_p^2 \cos^2(\beta)(K_{1mh} + K_{2mh})$$

$$+ K_{sp}]\}\ \Psi_{2h} + \{r_{1s} \cos(\alpha_1)K_{1ms}\}\Psi_{1s} - \{r_B \cos(\alpha_1)K_{1ms}\}\Psi_{1B} + C_{2,2}\dot{Y}_1 + C_{2,1}\dot{X}_1$$

$$+ C_{2,3}\dot{X}_p + C_{2,4}\dot{Y}_p + C_{2,6}\dot{Y}_2 + C_{2,8}\dot{Y}_B + C_{2,9}\dot{Z}_1 + C_{2,10}\dot{Z}_2 + C_{2,11}\dot{Z}_p$$

$$+ C_{2,12}\dot{\Psi}_i + C_{2,13}\dot{\Psi}_{1h} + C_{2,14}\dot{\Psi}_{2h} + C_{2,15}\dot{\Psi}_{1s} + C_{2,17}\dot{\Psi}_B$$

$$= - \{[- K_{1mh} \cos(\beta) + (r_p^2 \cos^2(\beta)K_{1mh})/(r_p^2 \cos^2(\beta)(K_{1mh} + K_{2mh}) + K_{sp})]e_{1h}(t)$$

$$+ [(r_p \cos^2(\beta)\ K_{1mh}K_{2mh})/(r_p^2 \cos^2(\beta)(K_{1mh} + K_{2mh}) + K_{sp})]e_{2h}(t) - [K_{1ms} \cos(\alpha_1)]\ e_{1s}(t)\}$$

Appendix B

Dimensionless Analysis

The equations of motion are expressed in dimensionless forms using certain characteristic parameters inherent in the geartrain system. The characteristic parameters are

$\bar{E}_p$ length, where $\bar{E}_p$ is the mean value of the displacement element function of the pinion and helical compound gear

$1/\omega_p$ time, where ω_p is the pinion speed

$\bar{E}_p\bar{K}_{1mh}$ force, where $\bar{K}_{1mh}$ is the mean value of the time-varying mesh characteristic stiffness of the pinion compound mesh

$(\bar{E}_p\bar{K}_{1mh})r_p$ torque, where r_p is the pinion base circle radius

$\bar{E}_p/r_p$ angle

The preceding characteristic parameters were used to define the following dimensionless parameters:

ωt time

Displacement/$\bar{E}_p$ linear displacement

$r_p/\bar{E}_p$ angular displacement

$M\omega_p^2/\bar{K}_{1mh}$ inertia in linear displacement equation

$I\omega_p^2/r_p^2\bar{K}_{1mh}$ inertia in angular displacement equation

$\omega_p C/\bar{K}_{1mh}$ damping of linear displacement in linear equation of motion

$\omega_p C/r_p\bar{K}_{1mh}$ damping of linear displacement in angular equation of motion

$\omega_p C/r_p\bar{K}_{1mh}$ damping of angular displacement in linear equation of motion

$\omega_p C/r_p^2\bar{K}_{1mh}$ damping of angular displacement in angular equation of motion

$K(t)/\bar{K}_{1mh}$ stiffness of linear displacement in linear equation of motion

$K(t)/r_p\bar{K}_{1mh}$ stiffness of linear displacement in angular equation of motion

$K(t)/r_p\bar{K}_{1mh}$ stiffness of angular displacement in linear equation of motion

$K(t)/r_p^2\bar{K}_{1mh}$ stiffness of angular displacement in angular equation of motion

Force/$(\bar{E}_p\bar{K}_{1mh})$ force

Torque/$(r_p\bar{E}_p\bar{K}_{1mh})$ torque

These dimensionless parameters were employed to carry out a computer simulation of the dynamics of this geartrain.

Appendix C

Calculations to Determine Spur Mesh Stiffness

The output from the GEARDYNMULT program is presented herein. The calculations to determine spur mesh stiffness were performed for the NASA Lewis split torque rig spur mesh. The nominal dimensions from engineering prints were used for the calculations. The output file from GEARDYNMULT follows:

SUN-PLANET MESH

ROTATIONAL PLANE
INVOLUTE MODIFICATIONS
****

(ENGAGEMENT)

PINION

LOC.	INV. MODIFIC.		DIA.	ROLL ANG.
	MIN.	MAX.		
0.0	0.000000	0.000000	2.7000	26.7174
0.1	0.000000	0.000000	2.6836	25.7954
0.2	0.000000	0.000000	2.6677	24.8734
0.3	0.000000	0.000000	2.6522	23.9514
0.4	0.000000	0.000000	2.6373	23.0295
0.5	0.000000	0.000000	2.6229	22.1074
0.6	0.000000	0.000000	2.6090	21.1855
0.7	0.000000	0.000000	2.5956	20.2635
0.8	0.000000	0.000000	2.5827	19.3415
0.9	0.000000	0.000000	2.5704	18.4195
1.0	0.000000	0.000000	2.5586	17.4974

GEAR

LOC.	INV. MODIFIC.		DIA.	ROLL ANG.
	MIN.	MAX.		
0.0	0.000000	0.000000	17.6000	26.7173
0.1	0.000000	0.000000	17.6167	26.8587
0.2	0.000000	0.000000	17.6334	27.0002
0.3	0.000000	0.000000	17.6502	27.1416
0.4	0.000000	0.000000	17.6671	27.2832
0.5	0.000000	0.000000	17.6841	27.4245
0.6	0.000000	0.000000	17.7011	27.5659
0.7	0.000000	0.000000	17.7182	27.7074
0.8	0.000000	0.000000	17.7354	27.8488
0.9	0.000000	0.000000	17.7527	27.9903
1.0	0.000000	0.000000	17.7700	28.1316

(DISENGAGEMENT)

PINION

LOC.	INV. MODIFIC.		DIA.	ROLL ANG.
	MIN.	MAX.		
0.0	0.000000	0.000000	2.7000	26.7174

```
0.1   0.000000   0.000000      2.7202   27.8188
0.2   0.000000   0.000000      2.7411   28.9203
0.3   0.000000   0.000000      2.7626   30.0218
0.4   0.000000   0.000000      2.7847   31.1233
0.5   0.000000   0.000000      2.8075   32.2247
0.6   0.000000   0.000000      2.8309   33.3262
0.7   0.000000   0.000000      2.8548   34.4278
0.8   0.000000   0.000000      2.8793   35.5292
0.9   0.000000   0.000000      2.9044   36.6307
1.0   0.000000   0.000000      2.9300   37.7323
```

GEAR

LOC.	INV. MODIFIC. MIN.	MAX.	DIA.	ROLL ANG.
0.0	0.000000	0.000000	17.6000	26.71731
0.1	0.000000	0.000000	17.5802	26.54831
0.2	0.000000	0.000000	17.5604	26.37931
0.3	0.000000	0.000000	17.5408	26.21031
0.4	0.000000	0.000000	17.5213	26.04141
0.5	0.000000	0.000000	17.5019	25.87241
0.6	0.000000	0.000000	17.4826	25.70351
0.7	0.000000	0.000000	17.4634	25.53451
0.8	0.000000	0.000000	17.4443	25.36541
0.9	0.000000	0.000000	17.4253	25.19651
1.0	0.000000	0.000000	17.4064	25.02751

I N P U T   D A T A

```
NO.TEETH -      SUN                                      27.0000
NO.TEETH - PLANET                                       176.0000
PRESSURE ANGLE (DEGREES) DRIVE SIDE                      25.0000
DIAMETRAL PITCH                                          10.0000
TOOTH TIP RADIUS TOL. (INCH)                              0.0020
EDGE BREAK ON TOPLAND (INCH)                              0.0100
MACHINED BACKLASH TOL.(INCH)                              0.0020
ROOT RADIUS TOL.        (INCH)                            0.0050
FACE WIDTH - SUN        (INCH)                            2.6000
FACE WIDTH - PLANET     (INCH)                            2.3600
YOUNGS MOD.*E-6 - SUN      (LB/SQ.INCH)                  30.0000
YOUNGS MOD.*E-6 - PLANET (LB/SQ.INCH)                    30.0000
POISSONS RATIO  - SUN                                     0.3000
POISSONS RATIO  - PLANET                                  0.3000
SURFACE ROUGHNESS-MAX (AA)                               25.0000
OIL INLET TEMPERATURE (DEG.F)                           180.0000
INITIAL RPM OF RANGE                                   2265.0000
FINAL RPM OF RANGE                                     2265.0000
NUMBER OF INTERVALS                                       1.0000
TORQUE INPUT (IN-LBS)                                  6960.0000
TOTAL INV.PROFILE MODIFICATION,ENGAGE (INCH)             0.0000
TOTAL INV.PROFILE MODIFICATION,DISENG (INCH)             0.0000
INV.PROFILE MOD.LOCATION-% OF SOE                        0.0000
INV.PROFILE MOD.LOCATION-% OF SOD                        0.0000
INV.PROFILE MOD.TOTAL TOLERANCE                          0.0000
+C.D.TOL. (OUT OF MESH)    (INCH)                        0.0000
-C.D.TOL. (INTO    MESH)   (INCH)                        0.0000
CONTACT RATIO INPUT                                      0.0000
HERTZ CONSTANT FOR COMPLIANCE                          159899.
CENTER DISTANCE,THEO. (INCH)                            10.1500
CENTER DISTANCE,MAX.  (INCH)                            10.1500
CENTER DISTANCE,MIN.  (INCH)                            10.1500
CIRCULAR PITCH        (INCH)                             0.3142
```

```
CIRCULAR BASE PITCH    (INCH)                       0.2847
MAX.OPERATING PRESS. ANGLE (DEG) DRIVE             25.0000
MIN.OPERATING PRESS. ANGLE (DEG) DRIVE             25.0000
NOMINAL CONTACT RATIO AT C.D.-THEO.                 1.5176
MINIMUM CONTACT RATIO AT C.D.-MAX.                  1.3443
MATERIAL CONSTANT                                   0.0528
CODE FOR TYPE OF OIL                                0.0000


Calculated Data

                                                    SUN       PLANET

NUMBER OF TEETH                                   27.0000  176.0000
PITCH DIAMETER                   (INCH)            2.7000   17.6000
BASE CIRCLE DIA. DRIVE SIDE      (INCH)            2.4470   15.9510
TOOTH TIP DIAMETER,MAX.          (INCH)            2.9300   17.7700
TOOTH TIP DIAMETER,MIN.          (INCH)            2.9260   17.7660
EFFECTIVE TOOTH TIP DIA          (INCH)            2.9060   17.7460
ROOT DIAMETER,MAX.               (INCH)            2.4976   17.3522
ROOT DIAMETER,MIN.               (INCH)            2.4876   17.3423
TRUE INV.FORM DIA.               (INCH)            2.5586   17.4064
TOPLAND WIDTH,MIN.               (INCH)            0.0475    0.0602
ROOT FILLET RADIUS,MIN.          (INCH)            0.0381    0.0401
MACHINE BACKLASH,MAX.            (INCH)            0.0025    0.0025
MACHINE BACKLASH,MIN.            (INCH)            0.0005    0.0005
CIRCULAR TOOTH THICKNESS         (INCH)            0.1711    0.1431
MACH.CIRC.TOOTH THKNS.MAX.       (INCH)            0.1706    0.1426
MACH.CIRC.TOOTH THKNS.MIN.       (INCH)            0.1686    0.1406
TIP/ROOT CLEAR.MIN AT CD MIN.    (INCH)            0.0162    0.0089
ROLL ANGLE AT TOOTH TIP DIA.     (DEG)            37.7323   28.1317
   ROLL ANGLE                    (DEG)            26.7174   26.7174
AT ADD.INV.MODIFICATION DIA.     (INCH)            2.7000   17.6000
ROLL ANGLE AT PITCH DIA.         (DEG)            26.7175   26.7174
   ROLL ANGLE                    (DEG)            26.7174   26.7174
AT DED.INV.MODIFICATION DIA.     (INCH)            2.7000   17.6000
ROLL ANGLE AT TIFD               (DEG)            17.4975   25.0276
INSPECTION WIRE/BALL DIA.               (INCH)     0.1650    0.1900
MAX.MEASUREMENT OVER 2 WIRE/BALL        (INCH)     2.9380   17.8709
MIN.MEASUREMENT OVER 2 WIRE/BALL        (INCH)     2.9342   17.8666
EFFECTIVE WIDTH AT TOOTH TIP                       2.6000    2.3600
EFFECTIVE WIDTH AT START OF FILLET                 2.6000    2.3600
RADIUS TO BASE OF FILLET INPUT (INCH)              0.0000    0.0000
OUTSIDE RADIUS INPUT    (INCH)                     0.0000    0.0000
FILLET RADIUS INPUT     (INCH)                     0.0000    0.0000
DAMPING RATIO INPUT                                0.0000    0.0000

NUMBER OF PLANETS                                    1
NUMBER OF BOUNDARY CONDITION ITERATIONS             20
TOLERANCE FOR BOUNDARY CONDITION CONVERGENCE  0.10000E-01
EQUIVALENT MASS OF SUN GEAR                   0.10000E+01
EQUIVALENT MASS OF PLANET CARRIER             0.10000E+01
EQUIVALENT MASS OF RING GEAR                  0.10000E+01
EQUIVALENT MASS OF PLANET # 1                 0.10000E+01

C O M P L I A N C E   C O N S T A N T S

   SUN-PLANET

  0.1379E-06 * ( 1 + -0.1229E+00 * (S/SO) +  0.5538E+00 * (S/SO)**2

            + -0.1054E+00 * (S/SO)**3 +  0.8697E-01 * (S/SO)**4)


C FORTRAN PROGRAM TO CALCULATE SPLIT TORQUE RIG
C TIME-VARYNG STIFFNESS FUNCTION FOR THE SPUR MESH
C
```

```
C
      DIMENSION A(8),SK(8)
C
      DO 11 J=1,495
      RJ=J
      X=14.+(13.333/245.)*RJ
C
C  CLEAR ARRAYS
C
      DO 12 K=1,8
      A(K)=0.
      SK(K)=0.
   12 CONTINUE
C
C CALC LOCAL COORDINATE ARRAY
C
      DO 13 K=1,8
      RK=K
      A(K)=X-(RK-1.)*13.333
   13 CONTINUE
C
C  CALC SLICE STIFFNESS ARRAY
C
      DO 14 K=1,8
      IF( A(K) .LT. -9.483 ) GOTO 117
      IF( A(K) .GT.  7.456 ) GOTO 117
      THETA=A(K)
      CALL LOA(S,THETA)
      CALL COMPL(S,C)
      SK(K)=1./C
  117 CONTINUE
   14 CONTINUE
      TK=0.
C
C LOOP TO CALC MESH STIFFNESS = SUM OF SLICE STIFFNESSES
C
      DO 15 K=1,8
      TK=TK+SK(K)
   15 CONTINUE
      WRITE(9,200) J,K,TK,TKM
   11 CONTINUE
  200 FORMAT(I5,F10.4,2E14.4)
      STOP
      END
C
C
C     SUBROUTINE COMPL (S,C)
C     VERSION 1.0
C     TIM KRANTZ  2/26/92
C
C     FORTRAN SUBROUTINE TO CALCULATE TOOTH STIFFNESS
C     COMPLIANCE KNOWING CORNELL'S COMPLIANCE COEFFICIENTS
C
C     REVISIONS:
C     VERSION 1.0  TIM KRANTZ  2/26/92
C
C
C     REQUIRED INPUTS:
C     S=LOCATION ALONG LINE OF ACTION
C
C     RETURNS:
C     COMP = COMPLIANCE OF TOOTH PAIR
C
```

```
C     ********************************************
C     ** NOTE:                                  **
C     ** 1) BY SETTING VALUES OF COEFFICIENTS   **
C     **     THE SUB IS SPECIFIC FOR A          **
C     **     PARTICULAR GEAR DESIGN.            **
C     ** 2) THE SUB IS NOT INTELLIGENT ABOUT    **
C     **     THE VALUE OF S.  IF YOU ASK IT     **
C     **     TO CALCULATE FOR A VALUE OF S      **
C     **     THAT REPRESENTS THE GEAR TOOTH     **
C     **     PAIR NOT IN CONTACT, IT WILL       **
C     **     FAITHFULLY CALCULATE A COMPLIANCE  **
C     **     ANYHOW.                            **
C     **                                        **
C     ********************************************
C
C
      SUBROUTINE COMPL(S,COMP)
C
C THE NEXT 5 FORTRAN STATEMENTS ARE SPECIFIC FOR A GIVEN DESIGN
C WHERE  A,B,C,D,C0 ARE COMPLIANCE COEFFICIENTS PER CORNELL
C AND S0=LENGTH OF LINE OF ACTION OVER ANGLE OF APPROACH
C
      S0=0.23084
      A=0.-0.1229
      B=0.5538
      C=0.-0.1054
      D=.8697E-01
      C0=0.1379E-06
      X=S/S0
      COMP=C0*(1+A*X+B*X*X+C*X*X*X+D*X*X*X*X)
      RETURN
      END
C   SUBROUTINE TO CALCULATE LINE OF ACTION
C   COORDINATE POSITION KNOWING THE LOCAL
C   ANGULAR COORDINATE THETA.
C   THIS SUBROUTINE IS FOR THE SPLIT TORQUE
C   HELICAL MESH GEOMETRY IN THE TRANSVERSE PLANE.
C   IT IS ASSUMED THAT BOTH S AND THETA ARE ZERO
C   AT THE PITCH POINT AND NEGATIVE ON THE ANGLE OF
C   APPROACH.  ALSO IT IS ASSUMED THAT THETA IS IN DEGRESS
C   AND IS WITHIN THE RANGE OF THE ANGLE OF APPROACH
C   THROUGH ANGLE OF RECESS
C
C   INPUTS : THETA IN DEGREES
C   OUTPUTS: S (INCHES)
C
      SUBROUTINE LOA(S,THETA)
      X=THETA*3.14159/180.
      S=0.9448*(TAN(.349292+X)-.364227)
      RETURN
      END
```

Appendix D

Calculations to Determine Helical Mesh Stiffness

The output from the GEARDYNMULT program is presented herein. The calculations to determine helical mesh stiffness were performed for the NASA Lewis split torque rig helical mesh. The gear dimensions used are those in the normal plane and were the nominal dimensions from engineering prints. The face widths used are 1/10 of the total face width because the helical gear was first modeled as 10 staggered spur gears. The output file from GEARDYNMULT follows:

```
                        SUN-PLANET MESH

                      ROTATIONAL   PLANE
                    INVOLUTE   MODIFICATIONS
                    ************************

                          (ENGAGEMENT)

                             PINION
```

LOC.	INV. MODIFIC.		DIA.	ROLL ANG.
	MIN.	MAX.		
0.0	0.000000	0.000000	2.0110	20.8652
0.1	0.000000	0.000000	2.0014	19.9960
0.2	0.000000	0.000000	1.9921	19.1267
0.3	0.000000	0.000000	1.9832	18.2574
0.4	0.000000	0.000000	1.9747	17.3882
0.5	0.000000	0.000000	1.9666	16.5191
0.6	0.000000	0.000000	1.9588	15.6499
0.7	0.000000	0.000000	1.9515	14.7807
0.8	0.000000	0.000000	1.9445	13.9114
0.9	0.000000	0.000000	1.9380	13.0422
1.0	0.000000	0.000000	1.9318	12.1728

```
                             GEAR
```

LOC.	INV. MODIFIC.		DIA.	ROLL ANG.
	MIN.	MAX.		
0.0	0.000000	0.000000	7.7927	20.8652
0.1	0.000000	0.000000	7.8025	21.0895
0.2	0.000000	0.000000	7.8125	21.3139
0.3	0.000000	0.000000	7.8225	21.5380
0.4	0.000000	0.000000	7.8327	21.7625
0.5	0.000000	0.000000	7.8429	21.9868
0.6	0.000000	0.000000	7.8532	22.2110
0.7	0.000000	0.000000	7.8636	22.4353
0.8	0.000000	0.000000	7.8741	22.6597
0.9	0.000000	0.000000	7.8847	22.8840
1.0	0.000000	0.000000	7.8954	23.1083

(DISENGAGEMENT)

PINION

| LOC. | INV. MODIFIC. | | DIA. | ROLL ANG. |
	MIN.	MAX.		
0.0	0.000000	0.000000	2.0110	20.8652
0.1	0.000000	0.000000	2.0235	21.9495
0.2	0.000000	0.000000	2.0366	23.0340
0.3	0.000000	0.000000	2.0502	24.1185
0.4	0.000000	0.000000	2.0643	25.2028
0.5	0.000000	0.000000	2.0790	26.2872
0.6	0.000000	0.000000	2.0942	27.3717
0.7	0.000000	0.000000	2.1098	28.4561
0.8	0.000000	0.000000	2.1260	29.5405
0.9	0.000000	0.000000	2.1426	30.6250
1.0	0.000000	0.000000	2.1597	31.7094

GEAR

| LOC. | INV. MODIFIC. | | DIA. | ROLL ANG. |
	MIN.	MAX.		
0.0	0.000000	0.000000	7.7927	20.86521
0.1	0.000000	0.000000	7.7805	20.58531
0.2	0.000000	0.000000	7.7685	20.30541
0.3	0.000000	0.000000	7.7566	20.02571
0.4	0.000000	0.000000	7.7449	19.74571
0.5	0.000000	0.000000	7.7333	19.46581
0.6	0.000000	0.000000	7.7219	19.18601
0.7	0.000000	0.000000	7.7106	18.90621
0.8	0.000000	0.000000	7.6995	18.62631
0.9	0.000000	0.000000	7.6885	18.34651
1.0	0.000000	0.000000	7.6777	18.06661

I N P U T   D A T A

NO.TEETH - SUN	32.0000
NO.TEETH - PLANET	124.0000
PRESSURE ANGLE (DEGREES) DRIVE SIDE	20.0100
DIAMETRAL PITCH	15.9123
TOOTH TIP RADIUS TOL. (INCH)	0.0020
EDGE BREAK ON TOPLAND (INCH)	0.0100
MACHINED BACKLASH TOL.(INCH)	0.0020
ROOT RADIUS TOL. (INCH)	0.0050
FACE WIDTH - SUN (INCH)	0.1750
FACE WIDTH - PLANET (INCH)	0.1500
YOUNGS MOD.*E-6 - SUN (LB/SQ.INCH)	30.0000
YOUNGS MOD.*E-6 - PLANET (LB/SQ.INCH)	30.0000
POISSONS RATIO - SUN	0.3000
POISSONS RATIO - PLANET	0.3000
SURFACE ROUGHNESS-MAX (AA)	25.0000
OIL INLET TEMPERATURE (DEG.F)	180.0000
INITIAL RPM OF RANGE	2265.0000
FINAL RPM OF RANGE	2265.0000
NUMBER OF INTERVALS	1.0000
TORQUE INPUT (IN-LBS)	695.6001
TOTAL INV.PROFILE MODIFICATION,ENGAGE (INCH)	0.0000
TOTAL INV.PROFILE MODIFICATION,DISENG (INCH)	0.0000
INV.PROFILE MOD.LOCATION-% OF SOE	0.0000
INV.PROFILE MOD.LOCATION-% OF SOD	0.0000
INV.PROFILE MOD.TOTAL TOLERANCE	0.0000
+C.D.TOL. (OUT OF MESH) (INCH)	0.0000

```
       -C.D.TOL. (INTO   MESH)    (INCH)              0.0000
       CONTACT RATIO INPUT                            0.0000
       HERTZ CONSTANT FOR COMPLIANCE                  306861.
       CENTER DISTANCE,THEO.  (INCH)                  4.9019
       CENTER DISTANCE,MAX.   (INCH)                  4.9019
       CENTER DISTANCE,MIN.   (INCH)                  4.9019
       CIRCULAR PITCH         (INCH)                  0.1974
       CIRCULAR BASE PITCH    (INCH)                  0.1855
       MAX.OPERATING PRESS. ANGLE (DEG) DRIVE        20.0100
       MIN.OPERATING PRESS. ANGLE (DEG) DRIVE        20.0100
       NOMINAL CONTACT RATIO AT C.D.-THEO.            1.7366
       MINIMUM CONTACT RATIO AT C.D.-MAX.             1.4258
       MATERIAL CONSTANT                              0.0528
       CODE FOR TYPE OF OIL                           0.0000

   Calculated Data
                                                SUN        PLANET


   NUMBER OF TEETH                            32.0000   124.0000
   PITCH DIAMETER              (INCH)          2.0110     7.7927
   BASE CIRCLE DIA. DRIVE SIDE (INCH)          1.8896     7.3223
   TOOTH TIP DIAMETER,MAX.     (INCH)          2.1597     7.8954
   TOOTH TIP DIAMETER,MIN.     (INCH)          2.1557     7.8914
   EFFECTIVE TOOTH TIP DIA     (INCH)          2.1357     7.8714
   ROOT DIAMETER,MAX.          (INCH)          1.8796     7.6284
   ROOT DIAMETER,MIN.          (INCH)          1.8696     7.6184
   TRUE INV.FORM DIA.          (INCH)          1.9318     7.6777
   TOPLAND WIDTH,MIN.          (INCH)          0.0410     0.0493
   ROOT FILLET RADIUS,MIN.     (INCH)          0.0279     0.0302
   MACHINE BACKLASH,MAX.       (INCH)          0.0025     0.0025
   MACHINE BACKLASH,MIN.       (INCH)          0.0005     0.0005
   CIRCULAR TOOTH THICKNESS    (INCH)          0.1071     0.0903
   MACH.CIRC.TOOTH THKNS.MAX.  (INCH)          0.1066     0.0898
   MACH.CIRC.TOOTH THKNS.MIN.  (INCH)          0.1046     0.0878
   TIP/ROOT CLEAR.MIN AT CD MIN.(INCH)         0.0144     0.0078
   ROLL ANGLE AT TOOTH TIP DIA. (DEG)         31.7094    23.1083
      ROLL ANGLE               (DEG)          20.8652    20.8652
   AT ADD.INV.MODIFICATION DIA. (INCH)         2.0110     7.7927
   ROLL ANGLE AT PITCH DIA.    (DEG)          20.8652    20.8652
      ROLL ANGLE               (DEG)          20.8652    20.8652
   AT DED.INV.MODIFICATION DIA. (INCH)         2.0110     7.7927
   ROLL ANGLE AT TIFD          (DEG)          12.1731    18.0666


   INSPECTION WIRE/BALL DIA.          (INCH)   0.1050     0.1150
   MAX.MEASUREMENT OVER 2 WIRE/BALL   (INCH)   2.1687     7.9476
   MIN.MEASUREMENT OVER 2 WIRE/BALL   (INCH)   2.1640     7.9423
   EFFECTIVE WIDTH AT TOOTH TIP                0.1750     0.1500
   EFFECTIVE WIDTH AT START OF FILLET          0.1750     0.1500


   RADIUS TO BASE OF FILLET INPUT (INCH)       0.0000     0.0000
   OUTSIDE RADIUS INPUT   (INCH)               0.0000     0.0000
   FILLET RADIUS INPUT    (INCH)               0.0000     0.0000
   DAMPING RATIO INPUT                         0.0000     0.0000

          NUMBER OF PLANETS                         1
          NUMBER OF BOUNDARY CONDITION ITERATIONS      20
          TOLERANCE FOR BOUNDARY CONDITION CONVERGENCE  0.10000E-01

          EQUIVALENT MASS OF SUN GEAR             0.10000E+01
          EQUIVALENT MASS OF PLANET CARRIER       0.10000E+01
          EQUIVALENT MASS OF RING GEAR            0.10000E+01
          EQUIVALENT MASS OF PLANET # 1           0.10000E+01

            C O M P L I A N C E   C O N S T A N T S
```

SUN-PLANET

0.2421E-05 * (1 + -0.2021E+00 * (S/SO) + 0.5166E+00 * (S/SO)**2

+ -0.3206E-01 * (S/SO)**3 + 0.1976E+00 * (S/SO)**4)

****** NON PLANETARY, NO CARRIER OR RING ******


```
C   PROGRAM TO CALCULATE SPLIT TORQUE RIG
C   TIME VARYING STIFFNESS FUNCTION FOR THE HELICAL MESH
C   HMESH1.FOR IS FOR HELIX ANGLE OF 6 DEGREES, ONLY
C   ONE LINE MUST BE CHANGED FOR A DIFFERENT HELIX ANGLE!
C
      DIMENSION A(240,23),SK(240,23),B(30),R(300)
C
      B(1)=6.
      B(2)=15.
      DO 734 MN=1,2
      AA=B(MN)*3.14159/180.
      XLF=0.356139*TAN(AA)
      DO 11 K=800,1025
      RK=K
      X=0.10*(RK-1.)
C
C   CLEAR ARRAYS
C
      DO 111 J=1,23
      DO 112 I=1,240
      A(I,J)=0.
      SK(I,J)=0.
  112 CONTINUE
  111 CONTINUE
C
C   CALC LOCAL COORDINATE ARRAY
C
      DO 113 J=1,23
      DO 114 I=1,240
      RI=I
      RJ=J
      A(I,J)=X-(RI-1.)*XLF-(RJ-1.)*11.25
  114 CONTINUE
  113 CONTINUE
C
C   CALC SLICE STIFFNESS ARRAY
C
      DO 115 J=1,23
      DO 116 I=1,240
      SK(I,J)=0.
      IF( A(I,J) .LT. -9.771 ) GOTO 117
      IF( A(I,J) .GT.  7.779 ) GOTO 117
      THETA=A(I,J)
      CALL LOA(S,THETA)
      CALL COMPL(S,C)
      SK(I,J)=1./(C*24.)
C
C   THE 24 IN THE STATEMENT ABOVE IS NEEDED BECAUSE THE SUBROUTINE
C   COMPL CALCULATES COMPLIANCE FOR A 1/10TH SLICE AND NOW I AM
C   DOING CALCS FOR 1/240TH SLICE - COMPLIANCE WILL BE 24 TIMES GREATER!
C
C     WRITE(8,400) I,J,THETA,S,SK(I,J)
  117 CONTINUE
  116 CONTINUE
  115 CONTINUE
```

```
          TK=0.
C 400 FORMAT(2I5,2F10.5,E14.4)
C
C  LOOP TO CALC MESH STIFFNESS = SUM OF SLICE STIFFNESS
C
      DO 118 J=1,23
      DO 119 I=1,240
      TK=TK+SK(I,J)
C     WRITE(8,100) I,J,A(I,J),SK(I,J)
  119 CONTINUE
  118 CONTINUE
      TKM=TK*175.118
      IF ( MN .EQ. 1) WRITE(8,200) X,TK,TKM
C     IF ( MN .EQ. 2) WRITE(9,200) X,TK,TKM
C     IF ( MN .EQ. 3) WRITE(10,200) X,TK,TKM
C     IF ( MN .EQ. 4) WRITE(11,200) X,TK,TKM
C     IF ( MN .EQ. 5) WRITE(12,200) X,TK,TKM
C     IF ( MN .EQ. 6) WRITE(13,200) X,TK,TKM
C     IF ( MN .EQ. 7) WRITE(14,200) X,TK,TKM
      write(6,333) MN,K
C     WRITE(8,200) X,TK,TKM
  333 format(2i5)
      R(K-799)=TK
   11 CONTINUE
      RMAX=R(1)
      RMIN=R(1)
      SUM=R(1)
      DO 227 KK=801,1025
      SUM=SUM+R(KK-799)
      IF( R(KK-799) .GT. RMAX) RMAX=R(KK-799)
      IF( R(KK-799) .LT. RMIN) RMIN=R(KK-799)
  227 CONTINUE
      SUM=SUM/225.
      DIFF=RMAX-RMIN
      PC=100*DIFF/SUM
      CR=1+7.59758*TAN(AA)
c     WRITE(8,300) B(MN),CR,PC
  734 CONTINUE
C 100 FORMAT(2I5,F10.5,E14.4)
  300 FORMAT(3F10.4)
  200 FORMAT(F10.5,2E14.4)
      STOP
      END
C
C    SUBROUTINE COMPL (S,C)
C    VERSION 1.0
C    TIM KRANTZ  2/26/92
C
C    FORTRAN SUBROUTINE TO CALCULATE TOOTH STIFFNESS
C    COMPLIANCE KNOWING CORNELL'S COMPLIANCE COEFFICIENTS
C
C    REVISIONS:
C    VERSION 1.0  TIM KRANTZ  2/26/92
C
C
C    REQUIRED INPUTS:
C    S=LOCATION ALONG LINE OF ACTION
C
C    RETURNS:
C    COMP = COMPLIANCE OF TOOTH PAIR
C
```

```
C     *********************************************
C     ** NOTE:                                   **
C     ** 1) BY SETTING VALUES OF COEFFICIENTS    **
C     **     THE SUB IS SPECIFIC FOR A           **
C     **     PARTICULAR GEAR DESIGN.             **
C     ** 2) THE SUB IS NOT INTELLIGENT ABOUT     **
C     **     THE VALUE OF S.  IF YOU ASK IT      **
C     **     TO CALCULATE FOR A VALUE OF S       **
C     **     THAT REPRESENTS THE GEAR TOOTH      **
C     **     PAIR NOT IN CONTACT, IT WILL        **
C     **     FAITHFULLY CALCULATE A COMPLIANCE   **
C     **     ANYHOW.                             **
C     **                                         **
C     *********************************************
C
C
      SUBROUTINE COMPL(S,COMP)
C
C     THE NEXT 5 FORTRAN STATEMENTS ARE SPECIFIC FOR A GIVEN DESIGN
C     WHERE  A,B,C,D,C0 ARE COMPLIANCE COEFFICIENTS PER CORNELL
C     AND S0=LENGTH OF LINE OF ACTION OVER ANGLE OF APPROACH
C
      S0=0.173406
      A=0.-0.2021
      B=0.5166
      C=0.-.03206
      D=0.1976
      C0=0.2421E-05
      X=S/S0
      COMP=C0*(1+A*X+B*X*X+C*X*X*X+D*X*X*X*X)
      RETURN
      END
C
C     SUBROUTINE TO CALCULATE LINE OF ACTION
C     COORDINATE POSITION KNOWING THE LOCAL
C     ANGULAR COORDINATE THETA.
C     THIS SUBROUTINE IS FOR THE SPLIT TORQUE
C     HELICAL MESH GEOMETRY IN THE TRANSVERSE PLANE.
C     IT IS ASSUMED THAT BOTH S AND THETA ARE ZERO
C     AT THE PITCH POINT AND NEGATIVE ON THE ANGLE OF
C     APPROACH.  ALSO IT IS ASSUMED THAT THETA IS IN DEGREES
C     AND IS WITHIN THE RANGE OF THE ANGLE OF APPROACH
C     THROUGH ANGLE OF RECESS
C
C     INPUTS : THETA IN DEGREES
C     OUTPUTS: S (INCHES)
C
      SUBROUTINE LOA(S,THETA)
      X=THETA*3.14159/180.
      S=0.9448*(TAN(.349292+X)-.364227)
      RETURN
      END
```

Appendix E

Calculations to Determine Input and Output Stiffnesses
and Inertias for Open-Loop Code

The data from the following tables were used in the calculations.

Torsional stiffness

Component	Stiffness, K, in.-lb/rad
Bull gear web, K_w	156.0×10^6
Torquemeter, K_{tq}	17.9
Bull gear shaft, K_{bg}	36.4
Compound shaft, K_{cs}	12.7
Pinion shaft, K_{ps}	0.71
High-speed shaft/coupling, K_{hs}	3.5

Mesh stiffness data

Component	Stiffness, K, lb/in.
Helical mesh, K_{hm}	5.7×16^6
Spur mesh, K_{sm}	8.5

Inertia data

Component	Inertia, I, lbm-in.^{2}
Torquemeter, I_{tq}	201
Drive motor, I_{dm}	4100
Bull gear, I_{bg}	466
Compound shaft, I_{cs}	11
Helical pinion, I_{hp}	1
High-speed shaft/coupling, I_{hs}	35

Total gear ratio of gearbox, GR ... 25.26
Base radius, in.
    Bull gear, R_{bg} 7.975
    Spur pinion, R_{sp} 1.224
    Helical gear, R_{hg} 0.944
    Helical pinion, R_{hp} 3.658

Apply the first rule: the kinetic energy of the output and input inertias of the analytical model should equal the kinetic energy of all the components not directly represented in the analytical model KE. Let θ represent the rotational speed of the component. Then

$$KE = \frac{1}{2} I_{dm}(\theta_{dm})^2 + \frac{1}{2} I_{bg}(\theta_{bg})^2 + \frac{1}{2} I_{tq}(\theta_{tq})^2$$

$$+ 2\left[\frac{1}{2} I_{cs}(\theta_{cs})^2\right] + \frac{1}{2} I_{hp}(\theta_{hp})^2 + \frac{1}{2} I_{hs}(\theta_{hs})^2$$

since

$$\theta_{bg} = \theta_{tq} = \theta_{dm}$$

$$\theta_{cs} = \theta_{dm} \cdot \frac{R_{bg}}{R_{sp}}$$

$$\theta_{hp} = \theta_{hs} = \theta_{dm} \cdot GR$$

Then

$$KE = \frac{1}{2} \left\{ (I_{dm} + I_{bg} + I_{tq})\theta_{dm}^2 + \left[2 I_{cs}\left(\frac{R_{bg}}{R_{sp}}\right)^2\right]\theta_{dm}^2 + (I_{hp} + I_{tq})(GR)^2\theta_{dm}^2 \right\}$$

or

$$KE = \frac{1}{2} \theta_{dm}^2 \cdot \left[I_{dm} + I_{bg} + I_{tq} + 2 I_{cs}\left(\frac{R_{bg}}{R_{sp}}\right)^2 + (I_{hp} + I_{tq}) \cdot (GR)^2\right]$$

Applying the data

$$KE = \theta_{dm}^2 \cdot (14\ 350\ \text{lbm-in.}^2)$$

so

$$KE = \theta_{dm}^2 \cdot (14\ 350) = \frac{1}{2}\left[I_o(\theta_o)^2 + I_i(\theta_i)^2\right]$$

since $\theta_i = \theta_o \cdot GR$ and $\theta_{dm} = \theta_o$,

$$KE = \theta_o^2 \cdot 14\ 350 = \frac{1}{2}\left(I_o\theta_o^2 + I_i \cdot GR^2 \cdot \theta_o^2\right)$$

Thus, the result of the first rule is

$$28\ 700 = I_o + I_i \cdot (25.26)^2$$

Apply the second rule: the ratio of the input inertia to the output inertia should equal the ratio of the stiffnesses of the two branches of the parallel path to the drive motor.

Path number 1 is the output shaft of the test gearbox to the drive motor:

$$K_1 = \left(\frac{1}{K_{bg}} + \frac{1}{K_{tq}} + \frac{1}{K_{bg}} \right)^{-1} = 9.02 \times 10^6 \text{ in.-lb/rad}$$

Path number 2 is the input shaft of the test gearbox (through the slave gearbox) to the drive motor:

Let
$$K_2 = \frac{U}{D}$$

where U is the unit torque at the test box pinion and D is the test box pinion rotation due to the deflection of all components in path 2.

Let
$$D = D_w + D_{sm} + D_{cs} + D_{hm} + D_{ps} + D_{hs} + D_{ps}$$

where D_w is the pinion rotation due to the deflection of K_w, and D_{sm} is the pinion rotation due to the deflection of K_{sm}, etc.

Then

$$D_{ps} = \frac{1}{K_{ps}}$$

$$D_{hs} = \frac{1}{K_{hs}}$$

$$D_{hm} = \frac{1}{2K_{hm}(R_{hp})^2}$$

$$D_{cs} = \frac{1}{2K_{cs}\left(\dfrac{R_{hp}}{R_{hg}}\right)^2}$$

$$D_{sm} = \frac{1}{2K_{sm}\left(\dfrac{R_{hp}R_{sp}}{R_{hg}}\right)^2}$$

$$D_w = \frac{(GR)^2}{K_w}$$

41

Substituting the numeric values,

$$K_2 = 1.18 \times 10^5 \text{ in.-lb/rad}$$

From the first rule,

$$28\ 700 = I_o + I_i(25.26)^2$$

From the second rule,

$$\frac{I_o}{K_1} = \frac{I_i}{K_2} \qquad \text{or} \qquad I_o = \frac{K_1}{K_2} I_i = \frac{9.02 \times 10^6}{1.18 \times 10^5} I_i$$

so

$$28\ 700 = \frac{9.02 \times 10^6}{1.18 \times 10^5} I_i + (25.26)^2 I_1$$

$$I_i = 40.2 \text{ lbm-in.}^2$$

$$I_o = 3070 \text{ lbm-in.}^2$$

References

1. Bossler, R.; and Heath, G.: Advanced Rotorcraft Transmission (ART) Program Status. Rotary Wing Propulsion Specialists' Meeting; Proceedings, American Helicopter Society, Alexandria, VA, 1990, 14 p.

2. Kish, J.: Advanced Rotorcraft Transmission (ART) Program Review. Rotary Wing Propulsion Specialists' Meeting; Proceedings, American Helicopter Society, Alexandria, VA, 1990, 11 p.

3. Lenski, J.: Boeing Helicopters Advanced Rotorcraft Transmission (ART) Program Status. Rotary Wing Propulsion Specialists' Meeting; Proceedings, American Helicopter Society, Alexandria, VA, 1990, 15 p.

4. White, G.: Design Study of Split-Torque Helicopter Transmissions. Submitted to NASA Lewis Research Center Under Contract NAS3–22528, 1982.

5. Cocking, H.: The Design of an Advanced Engineering Gearbox. Vertica, vol. 10, no. 2, 1986, pp. 213–215.

6. Smirnov, G: Multiple-Power-Path Nonplanetary Main Gearbox of the Mi-26 Heavy-Lift Transport Helicopter. Mil. Bureau, Moscow, Vertiflite, March/April, 1990, pp. 20–23.

7. Haller, W.; and Deeg, T.: Low Noise Marine Gears. Proceedings, 1991 AGMA Fall Technical Meeting, TP–91–FTM–4.

8. Sigg, H.: Marine Gearing—Development and Technology. Proc. Inst. Mech. Eng., vol. 204, Pt. A, 1990, pp. 3–14.

9. White, G.: New Family of High-Ratio Reduction Gear with Multiple Drive Paths. Proc. Inst. Mech. Eng., vol. 188, Pt. A, 1974, pp. 281–288.

10. White, G.: Design of A 375 KW Helicopter Transmission with Split-Torque Epicyclic and Bevel Drive Stages. Proc. Inst. Mech. Eng., vol. 197, Pt. C, 1983, pp. 213–224.

11. White, G.: A 2400 kW Lightweight Helicopter Transmission With Split-Torque Gear Trains. ASME Paper 84–Det–91, 1984.

12. White, G.: 3600 HP Split-Torque Helicopter Transmission. NASA CR–174932, 1985.

13. White, G.: Split-Torque Helicopter Transmission with Widely Separated Engines. Proc. Inst. Mech. Eng., vol. 203, Pt. A, 1989, pp. 53–65.

14. Hasiang-Hsi (Edward Lin); Huston, R.; and Coy, J.: On Dynamic Loads in Parallel Shaft Transmissions, I-Modeling and Analysis. NASA TM–100180, 1987.

15. Hasiang-Hsi (Edward Lin); Huston, R.; and Coy, J.: On Dynamic Loads in Parallel Shaft Transmissions, II—Parametric Study. NASA TM–100181, 1987.

16. Choy, F., et al.: Vibration Signature Analysis of Multistage Gear Transmission. NASA TM–101442, 1988.

17. Zakrajsek, J.: Comparison Study of Gear Dynamics Computer Programs at NASA Lewis Research Center. NASA TP–2901, 1989.

18. Buyukataman, K.: A New Approach for the Dynamic Loads of Heavily Loaded (d > e) High Speed Aircraft Gearing. Proceedings, 1988 AGMA Fall Technical Meeting, TP–88–FTM–5.

19. Zuerbes, A., et al.: Stability Behavior of Geared Rotor Systems Regarding Torsional Lateral Coupling. Rotating Machinery Dynamics; Proceedings of the Twelfth Biennial ASME Conference on Mechanical Vibration and Noise, ASME, NY, 1989, pp. 217–224.

20. Lin, H.; Oswald, F.; and Townsend, D.: Dynamic Loading of Spur Gears With Linear or Parabolic Tooth Profile Modifications, NASA TM–101444, 1988.

21. Kahraman, A., et al.: Dynamic Analysis of Geared Rotors by Finite Elements. NASA TM–102349, 1990.

22. Lin, H.; and Huston, R.: Dynamic Loading on Parallel Shaft Gears. NASA CR–179473, 1986.

23. Iwatsubo, T.; Arii, S.; and Kawai, R.: Coupled Lateral-Torsional Vibration of Rotor System Trained by Gears, Part 1, Analysis by Transfer Matrix Method. Bull. JSME, vol. 27, no. 224, Feb. 1984, pp. 271–277.

24. Ozguven, H.; and Houser, D.: Dynamic Analysis of High Speed Gears by Using Loaded Static Transmission Error. J. Sound Vib., vol. 125, 1988, pp. 71–83.

25. Mark, W.D.: Use of the Generalized Transmission Error in the Equations of Motion of Gear Systems. J. Mech. Trans. Autom. Des., vol. 109, 1987, pp. 283–291.

26. Cornell, R: Compliance and Stress Sensitivity of Spur Gear Teeth. J. Mech. Des., vol. 103, no. 2, Apr. 1981, pp. 447–459.

27. Savage, M., et al.: Gear Mesh Compliance Modeling. NASA TM–88843, 1986.

28. Munro, R.: The D.C. Component of Gear Transmission Error. Proceedings of The 1989 International Power Transmission and Gearing Conference, Vol. 1, ASME, New York, 1989, pp. 467–470.

29. Frater, J.; August, R.; and Oswald, F.: Vibration in Planetary Gear Systems With Unequal Planet Stiffness. NASA TM–83428, 1983.

30. Boyd, L.S.; and Pike, J.: Multi-Mesh Gear Dynamics Program Evaluation and Enhancements. NASA CR–174747, 1985.

31. Boyd, L.S.; and Pike, J.: Expansion of Epicyclic Gear Dynamic Analysis Program. NASA CR–179563, 1986.

32. Choy, F.K.; Townsend, D.P.; and Oswald, F.B.: Dynamic Analysis of Multimesh-Gear Helicopter Transmission. NASA TP–2789, 1988.

33. Hochmann, D., et al.: Transmission Error and Load Distribution Analysis of Spur and Double Helical Gear Pair Used in a Split Path Helicopter Transmission Design. AHS and Royal Aeronautical Society, Technical Specialists Meeting on Rotorcraft Acoustics/Fluid Dynamics, Philadelphia, PA, 1991, 14 p.

34. Rashidi, M.; and Krantz, T: Dynamics of a Split Torque Helicopter Transmission. NASA TM–105681, 1992.

35. IMSL User's Manual. IMSL Inc., 1991.

36. Boyd, L.: Two Stage Gear Tooth Dynamics Program. NASA CR–185110, 1989.

37. Singh, R.; and Lim, T.: Vibration Transmission Through Rolling Element Bearings in Geared Rotor Systems. NASA CR–4334, 1990.

38. Bibel G., et al.: Effects of Rim Thickness on Spur Gear Bending Stress. NASA TM–104388, 1991.

39. Benedict, G.; and Kelley, B.: Instantaneous Coefficients of Friction. Presented at the ASLE/ASME Lubrication Conference, 1960, preprint 60 LC–2.

40. Hamrock, B.: Fundamentals of Fluid Film Lubrication. NASA RP–1255, 1991.

Dual power path

Input power

(high speed)

Output power

(low speed)

Dual power path
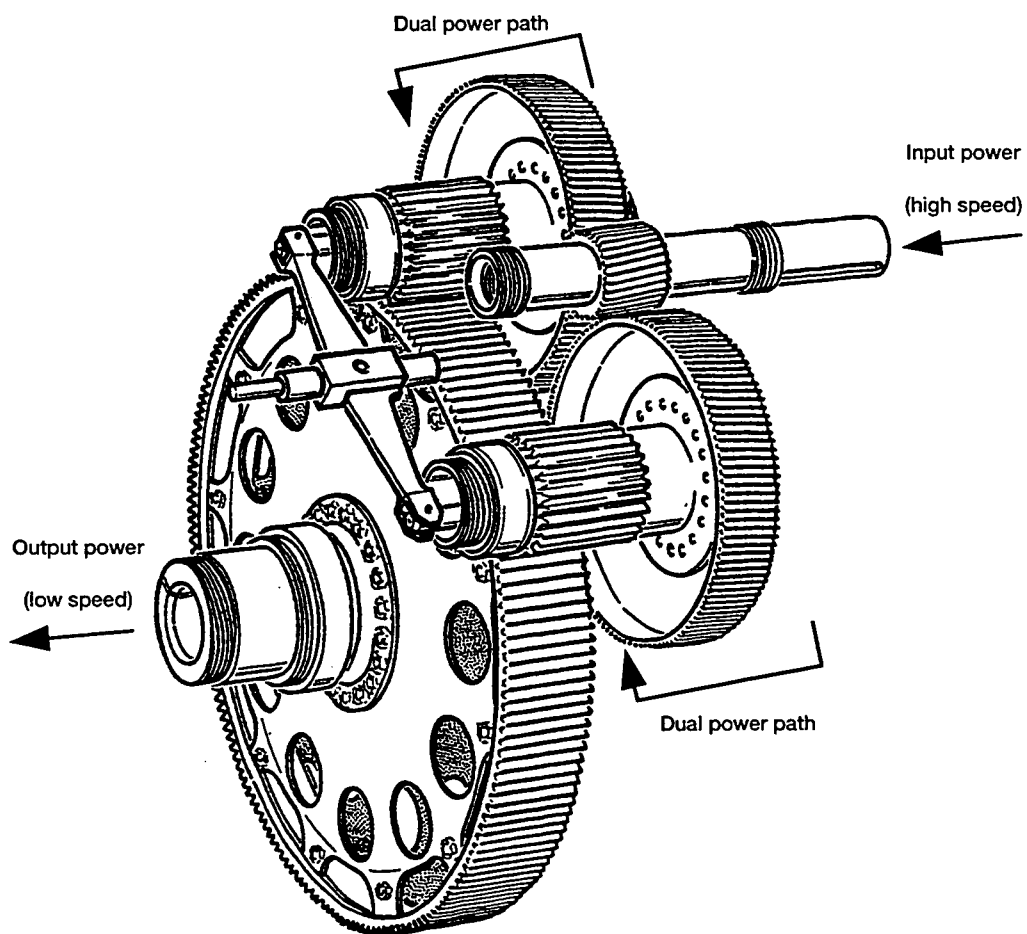
Figure 1.1.—Split torque design for helicopter application.
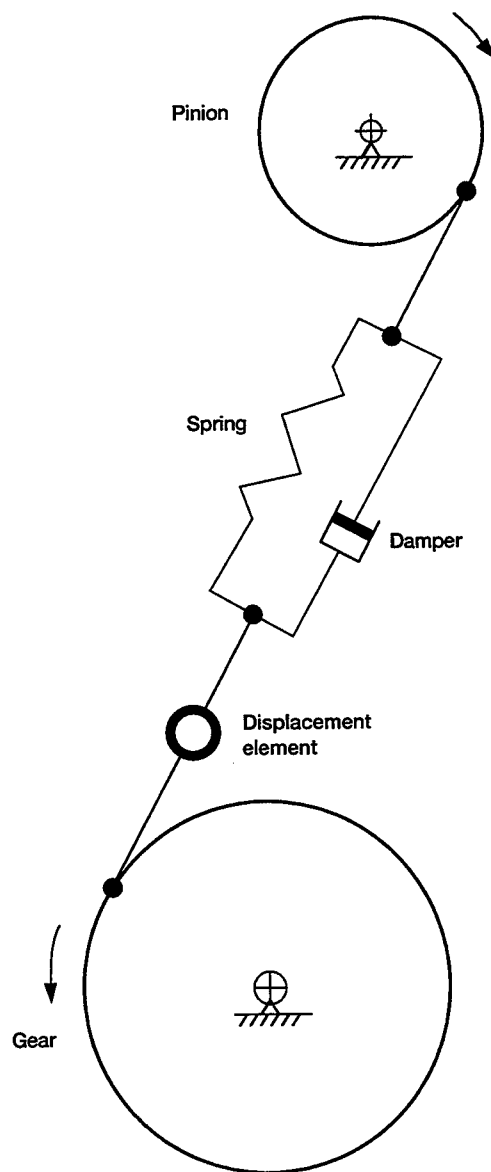
Figure 2.1.—Gear dynamics model.

47

Spur bull gear
500-hp output
at 347.5 rpm

Balance beam

Gear/pinion assembly
250 hp at 2230 rpm

Helical pinion
500-hp input
at 8780 rpm

C-90-04452
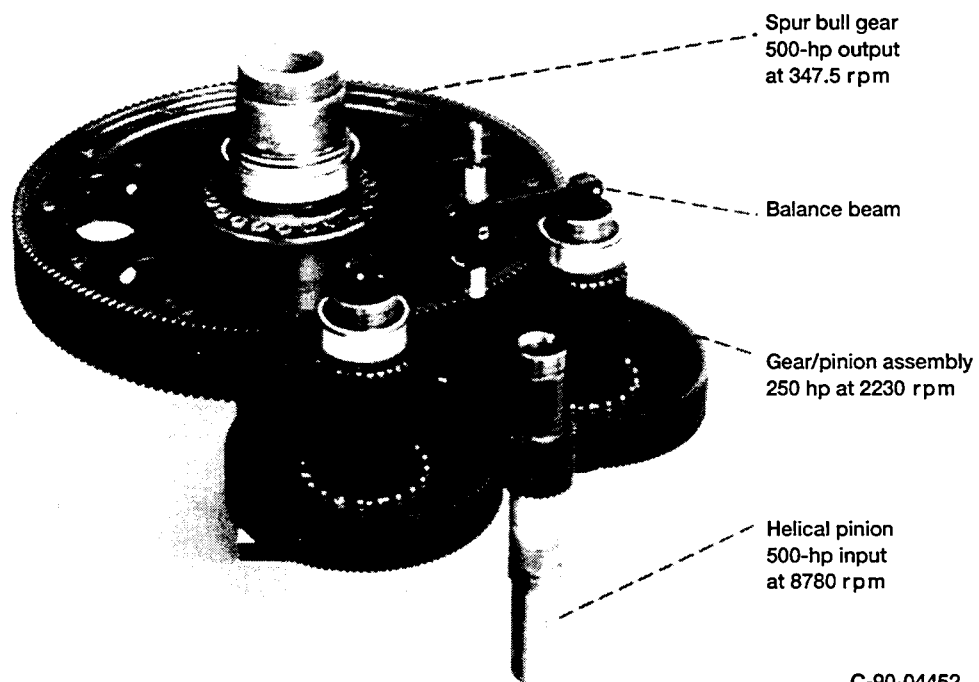
Figure 2.2.—Geartrain of split torque test gearbox.

Bull gear

α_B

α_1

α_2

α_p

First
compound
gear

Pinion

Second
compound
gear
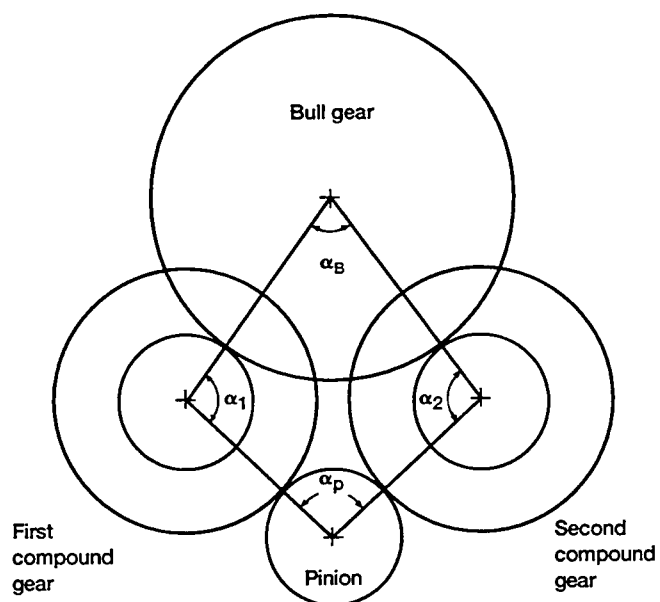
Figure 2.3.—Top view of gearbox showing shaft angles.

48
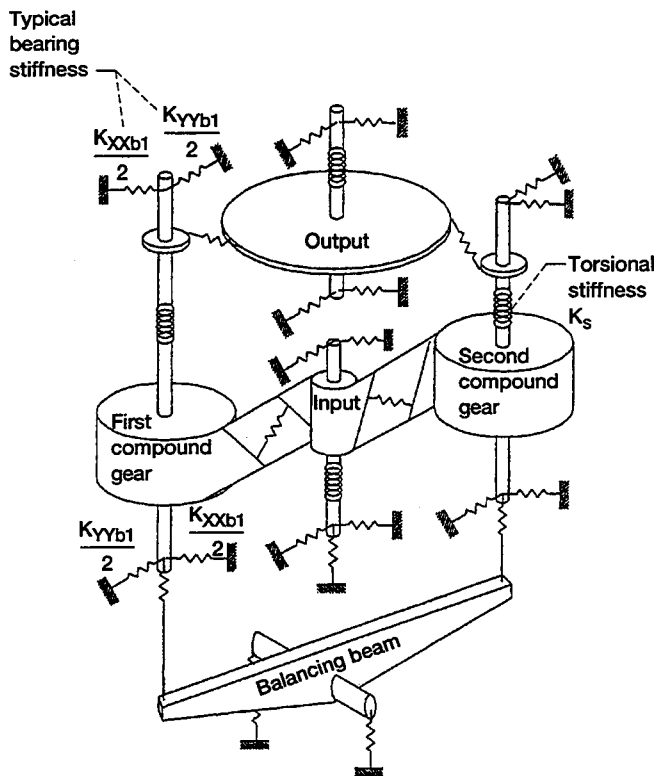
Figure 2.4.—Split torque model (Note: damping elements, input and output inertias not shown).
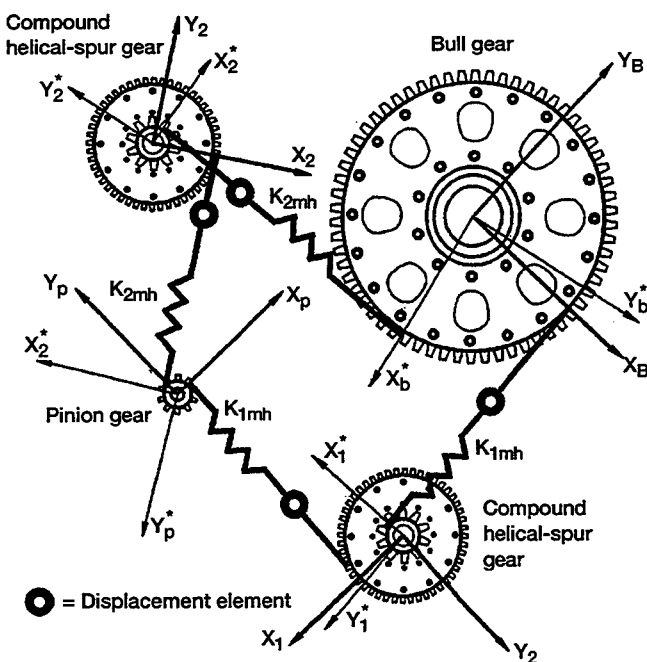
Figure 2.5.—Top view of analytical model showing global and local reference frames.
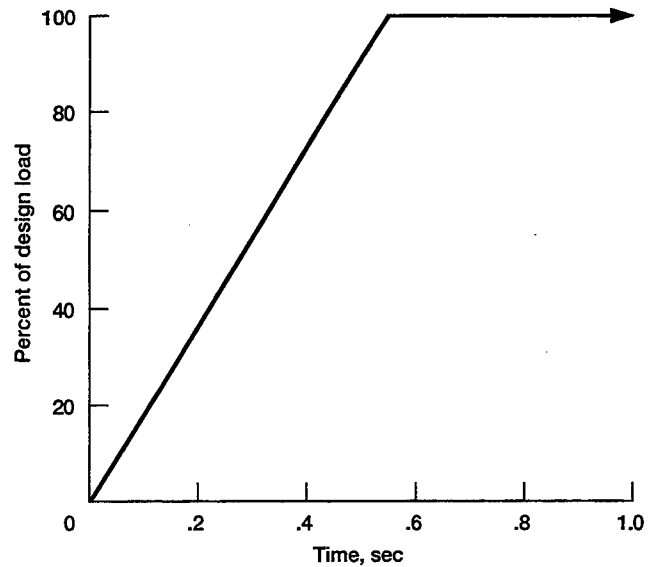
Figure 2.6.—Ramp shape loading function.
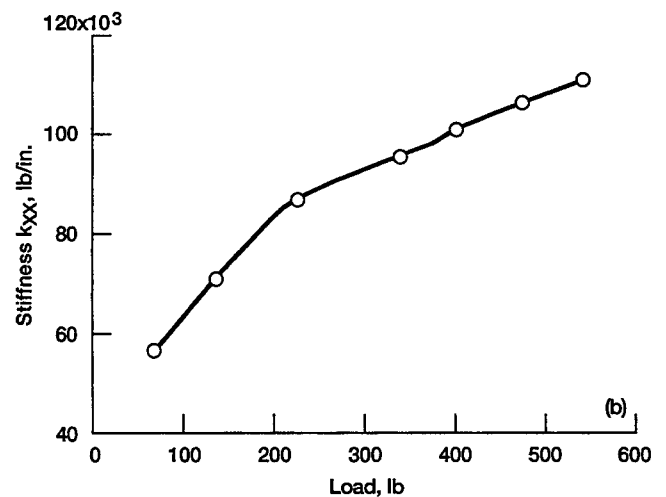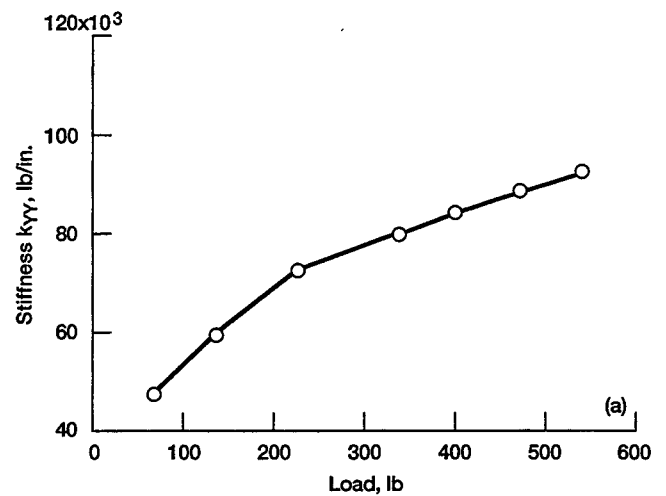
Figure 3.1.—Bearing stiffness as a function of load. (a) Stiffness perpendicular to load. (b) Stiffness parallel to load.

49
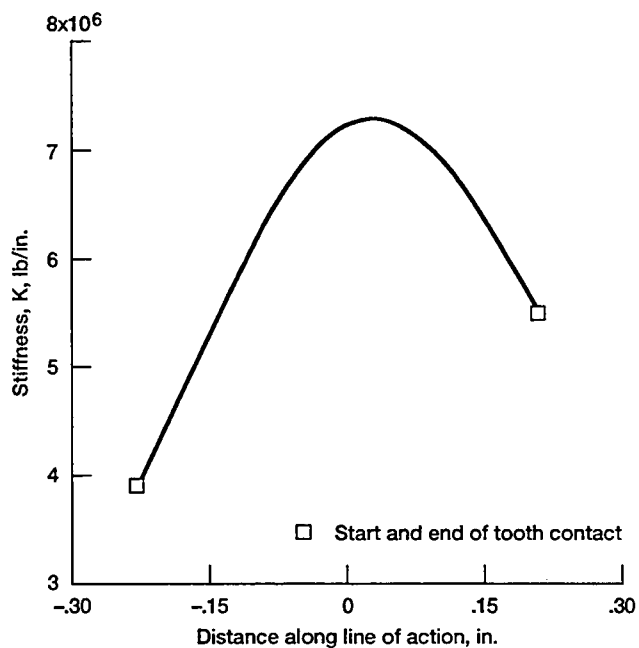
Figure 3.2.—Stiffness of single tooth pair for spur mesh.
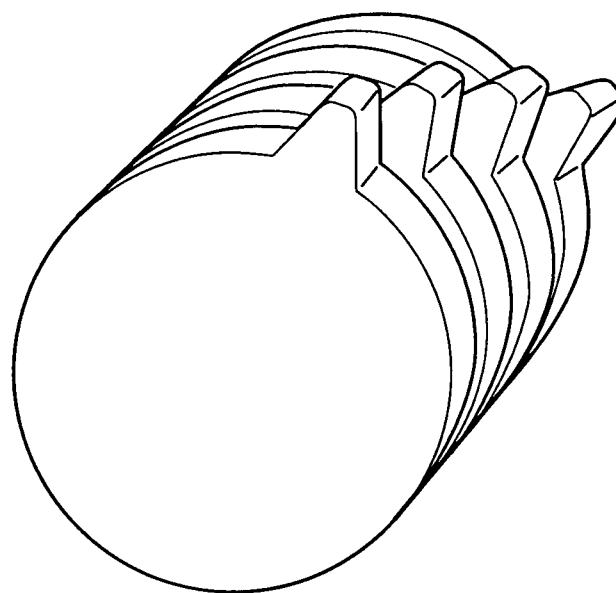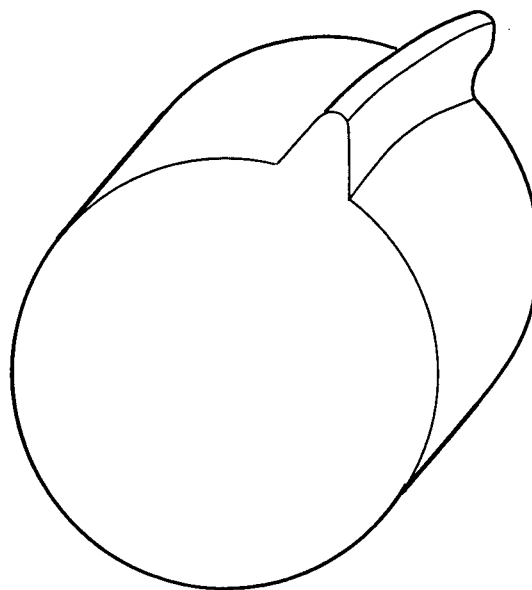
Figure 3.4.—Staggered spur gears to approximate a helical gear.
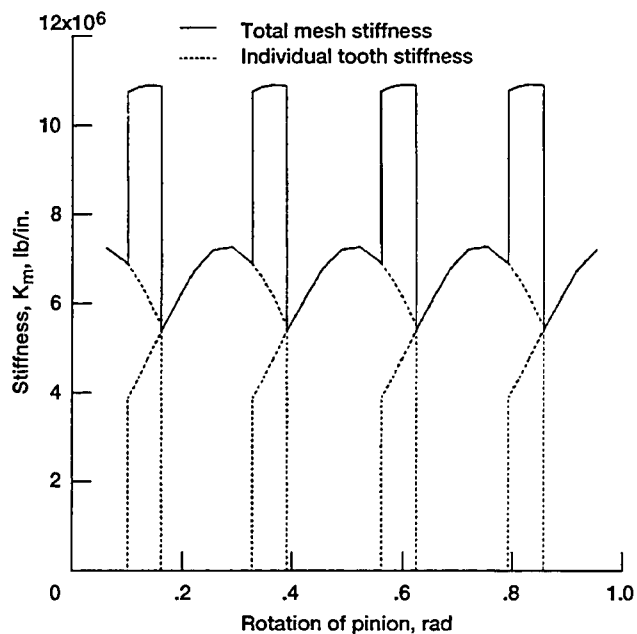
Figure 3.3.—Spur mesh stiffness variation.

50
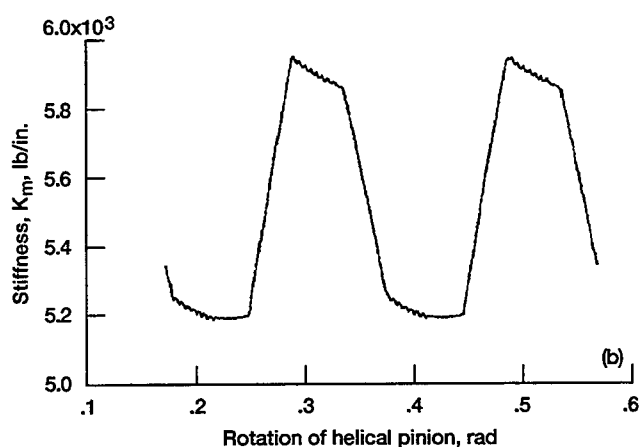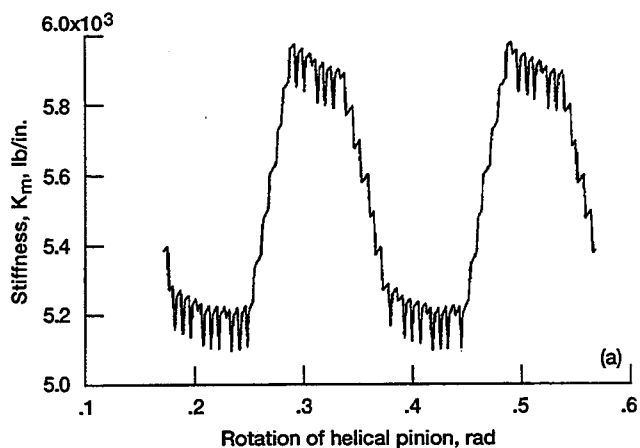
Figure 3.5.—Helical mesh stiffness variation by staggered spur gear approximation. (a) 24 spur gear slices per helical gear. (b) 240 spur gear slices per helical gear.
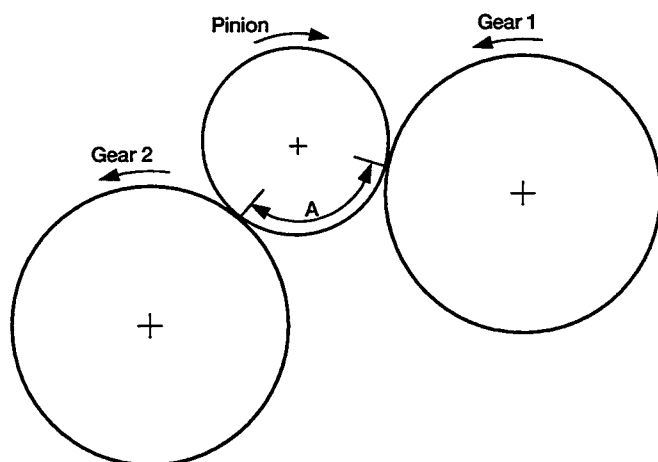
A = arc length defining phase relationship

Figure 3.6.—Arc length that defines mesh phasing relationship.
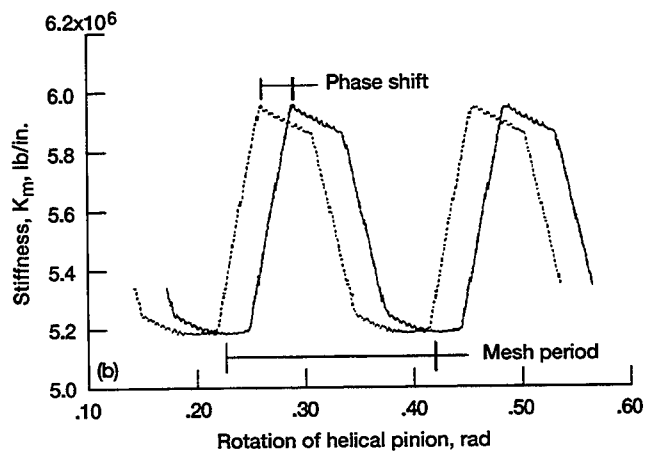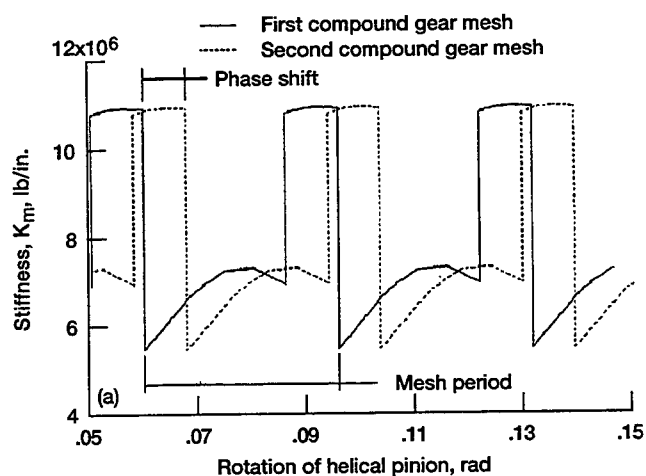
Figure 3.7.—Phase relationships of mesh stiffness functions. (a) Spur mesh. (b) Helical mesh.
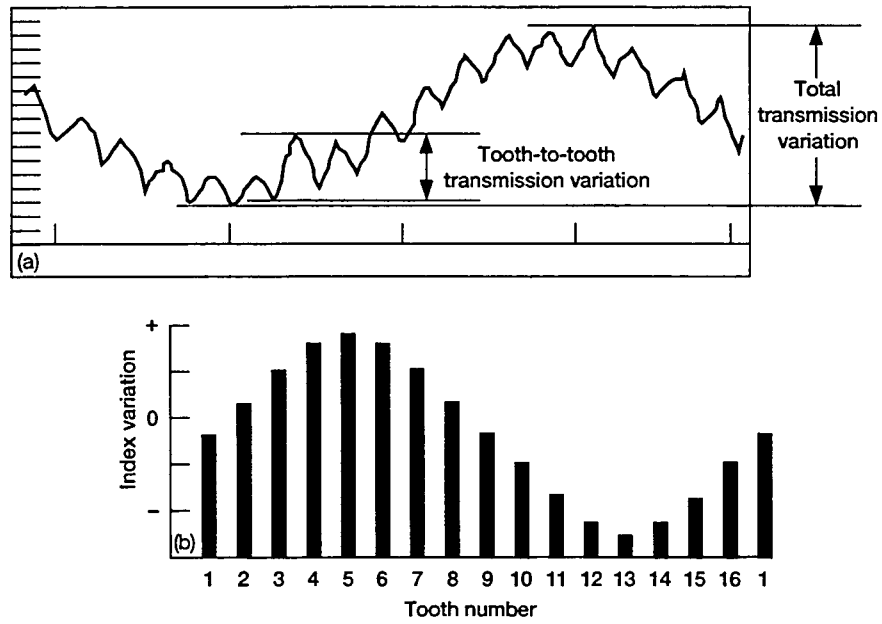
Figure 3.8.—Typical gear inspection measurements showing sinusoidal total transmission variation by (a) single flank and (b) index.
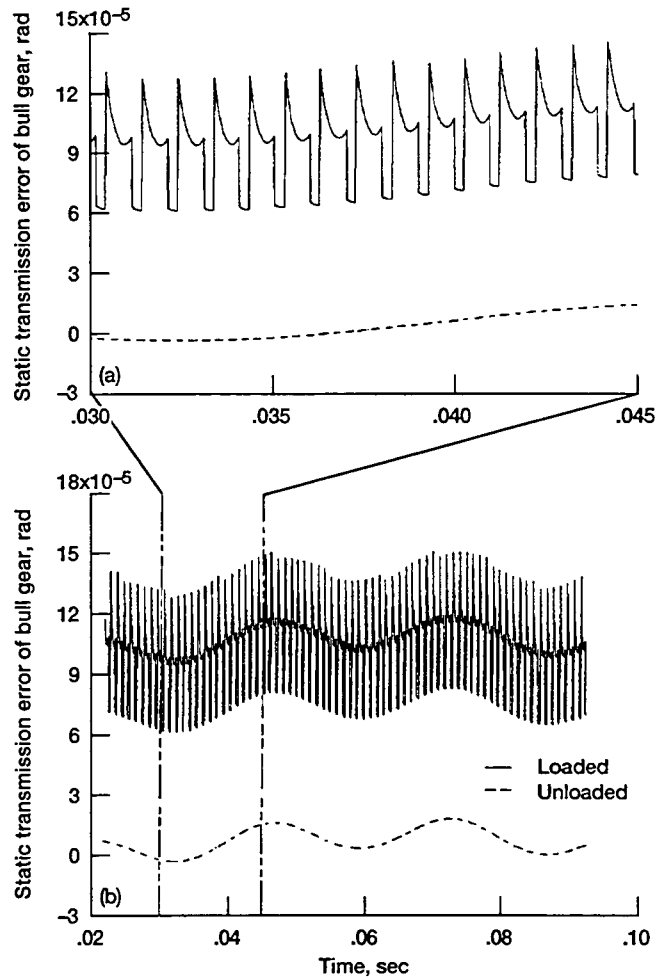
Figure 3.9.—Unloaded and loaded static transmission errors for spur mesh with rigid bearing supports. (a) Mesh period. (b) Gear period.

52
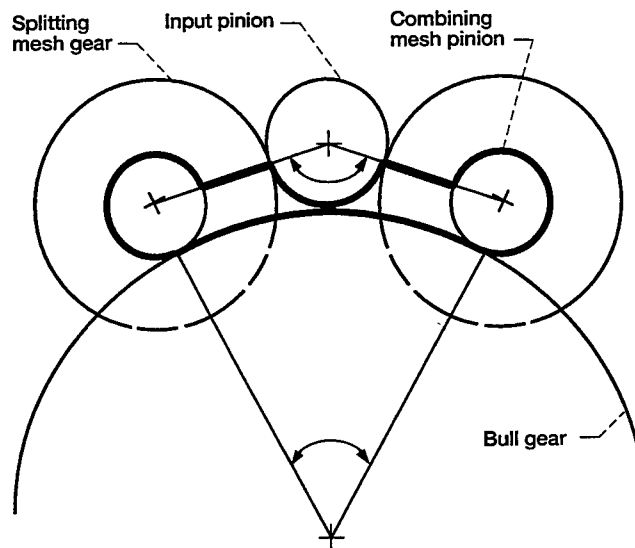
Figure 3.10.—Split torque arrangement with locked loop of gearing.
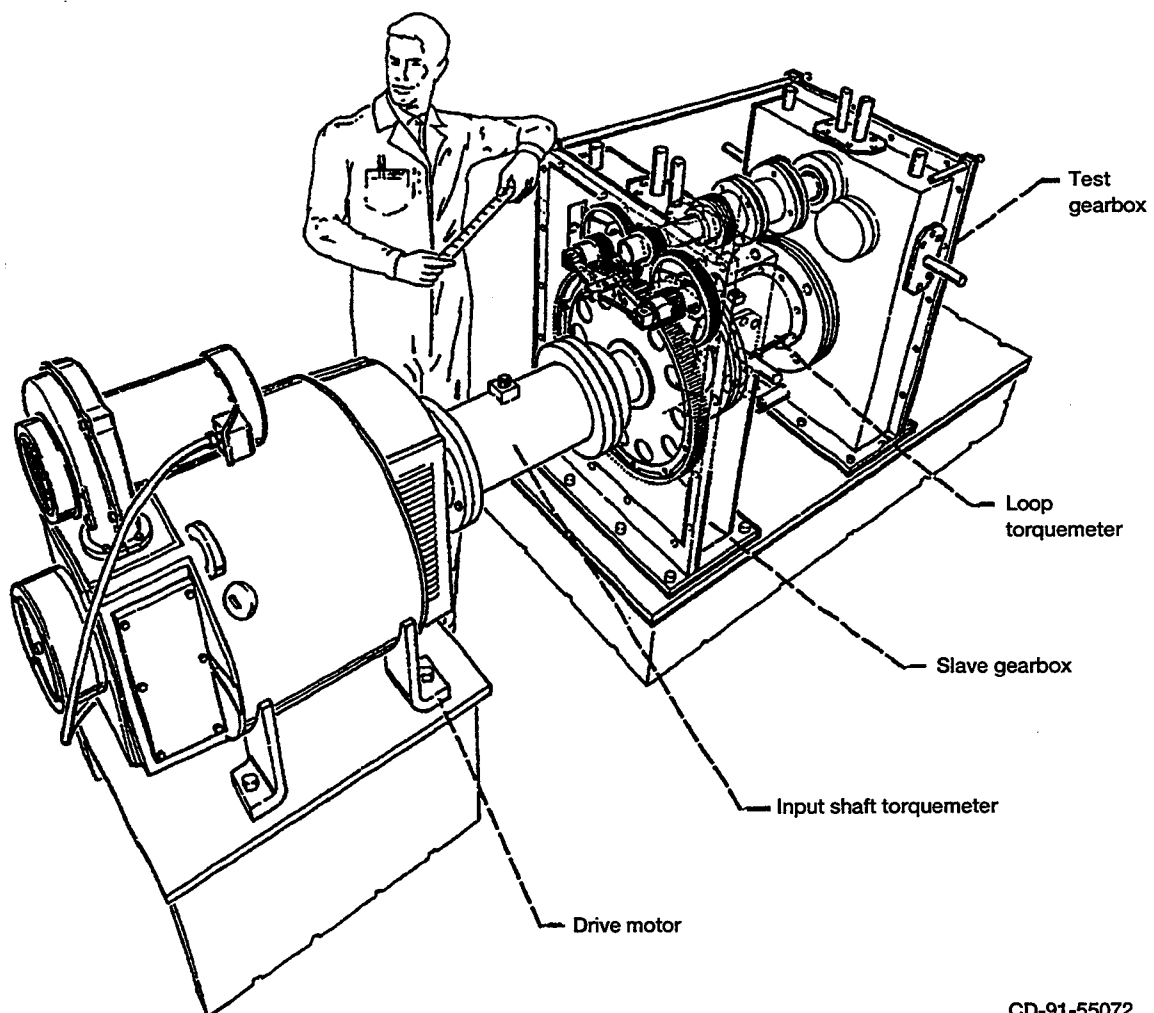
CD-91-55072

Figure 3.11.—Experimental split torque gearbox test facility.

53

(a)

Test gearbox
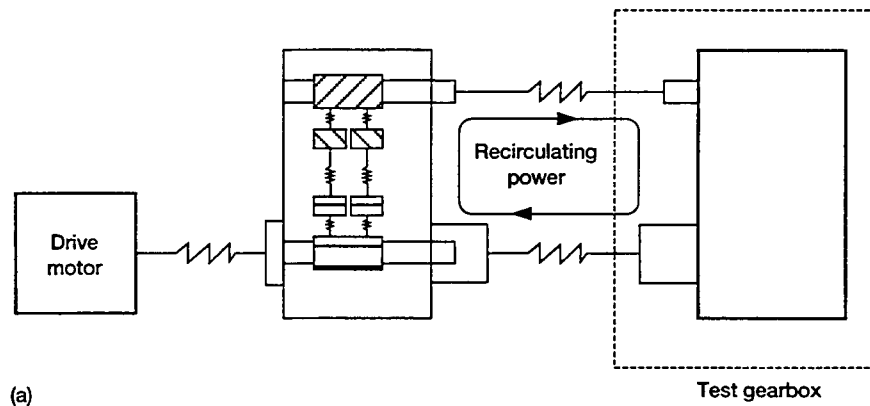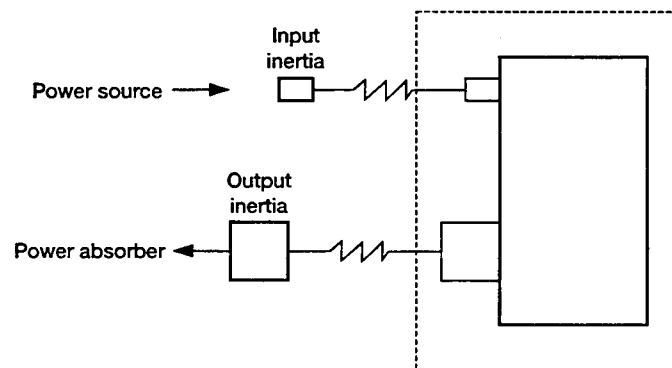
(b)

Figure 3.12.—Closed-loop system modeled as an open-loop system. (a) Experimental system, closed loop. (b) Analytical model, open loop.
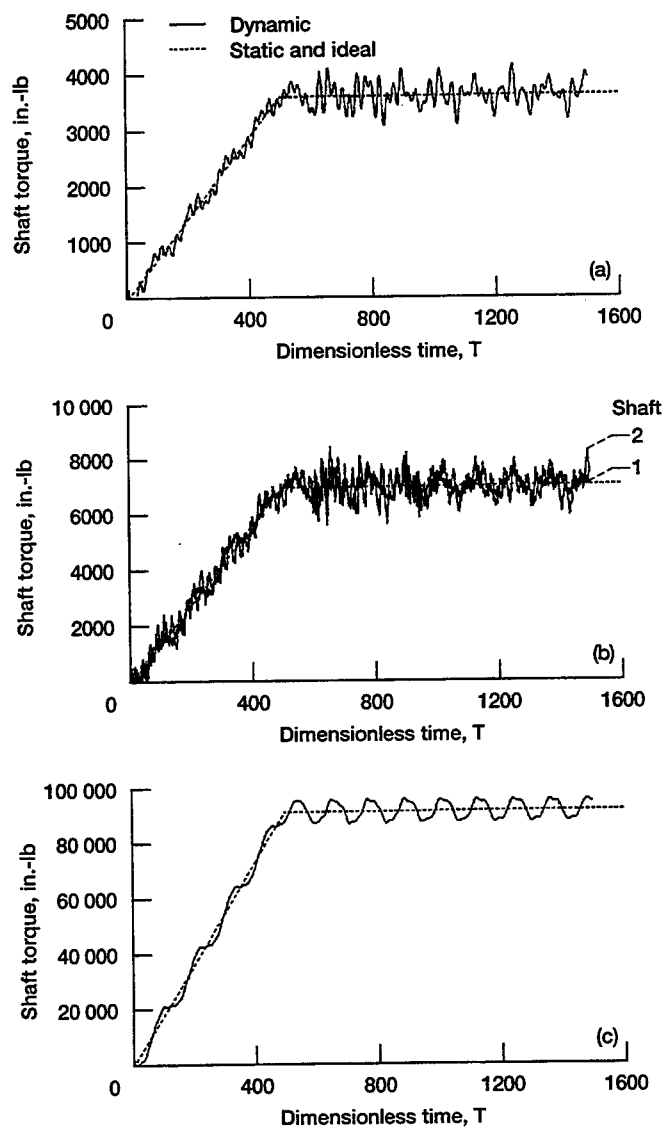
Figure 3.13.—Shaft torques for case 1, nominal conditions. (a) Input shaft. (b) Compound shafts. (c) Output shafts.
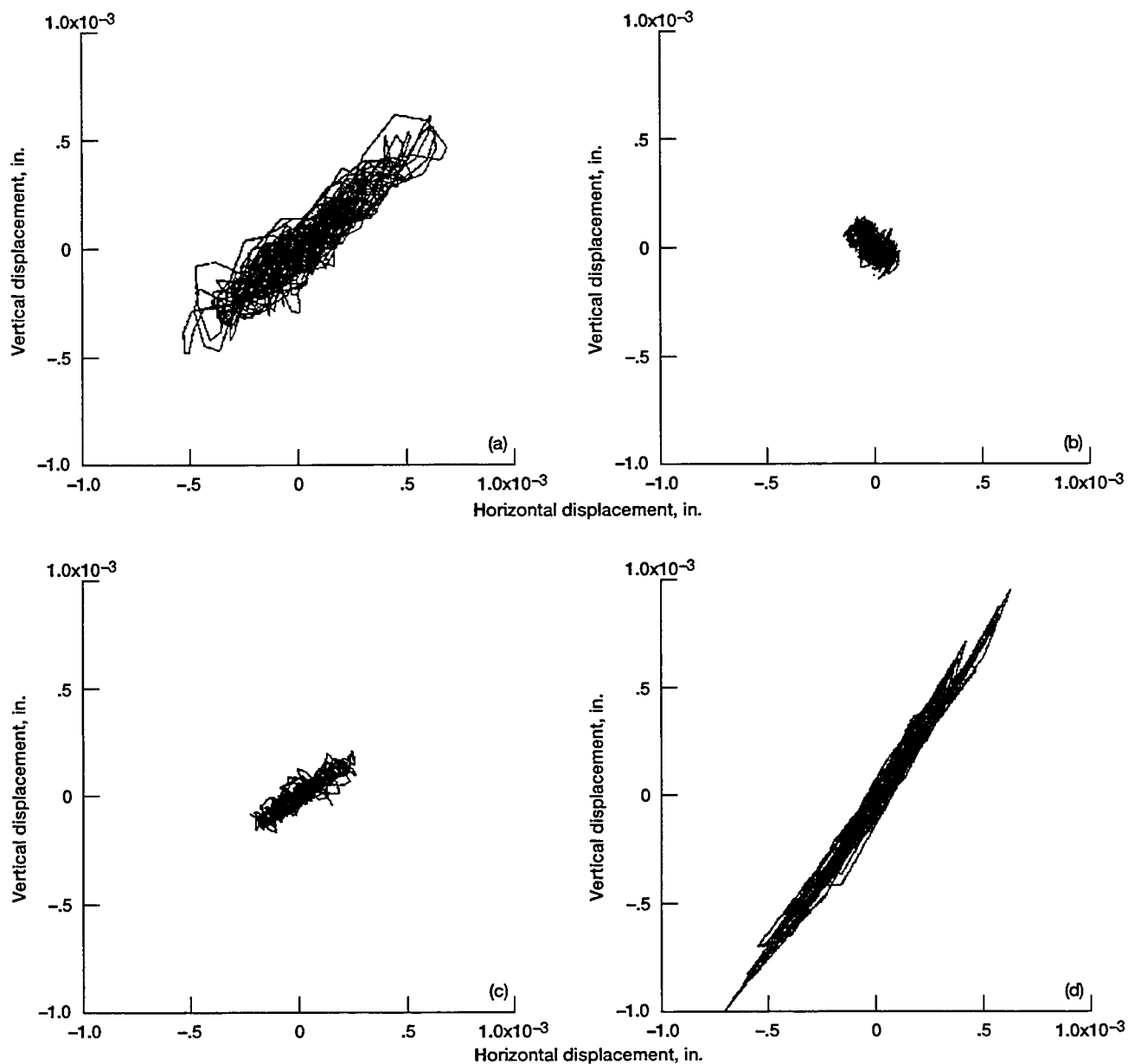
Figure 3.14.—Shaft orbits for case 1, nominal conditions. (a) Input pinion shaft. (b) Compound shaft 1. (c) Compound shaft 2. (d) Output gear shaft.
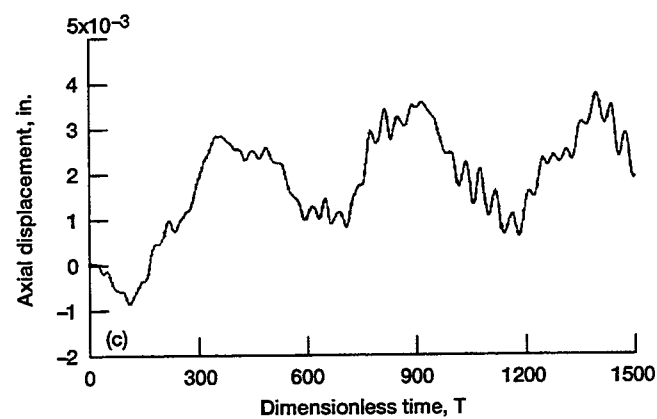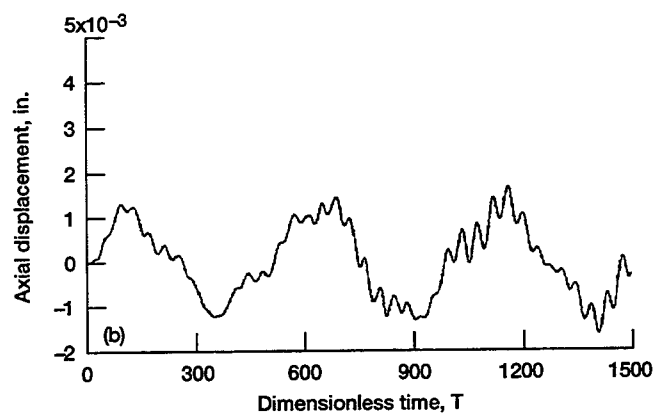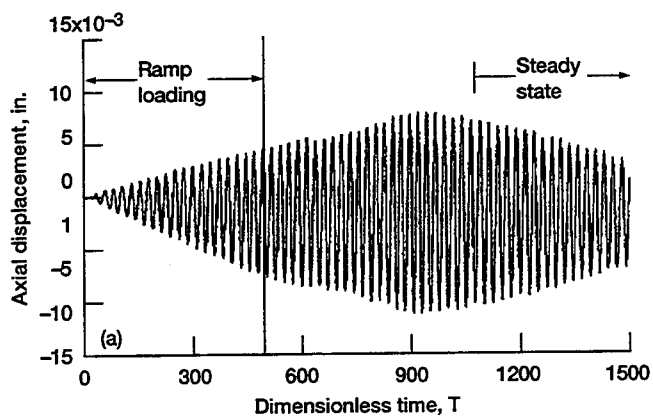
Figure 3.15.—Axial motions in absence of friction. (a) Input pinion shaft. (b) Compound shaft 1. (c) Compound shaft 2.
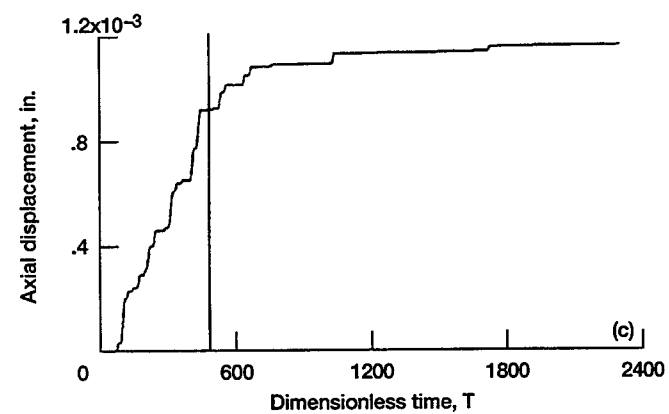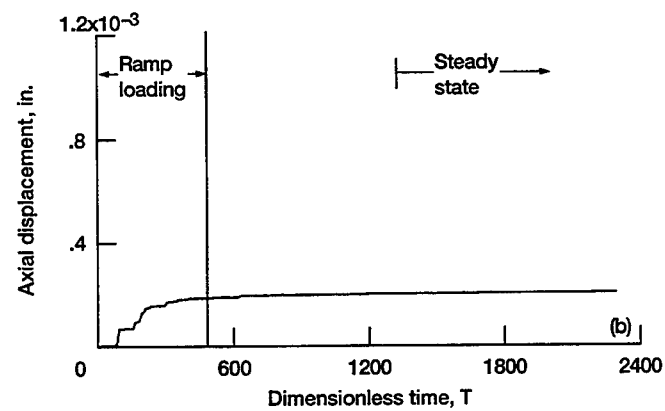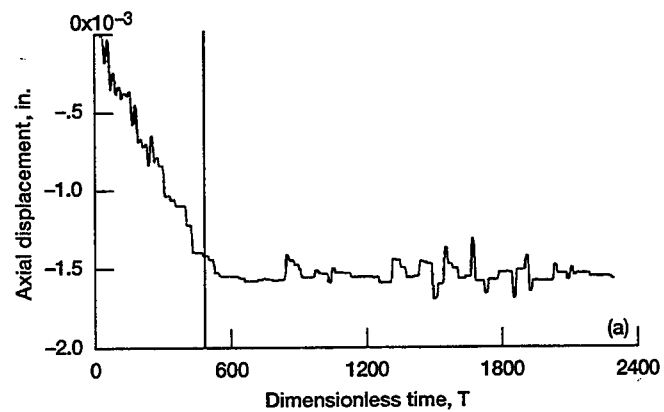
Figure 3.16.—Axial motions in presence of friction. (a) Input pinion shaft. (b) Compound shaft 1. (c) Compound shaft 2.

57
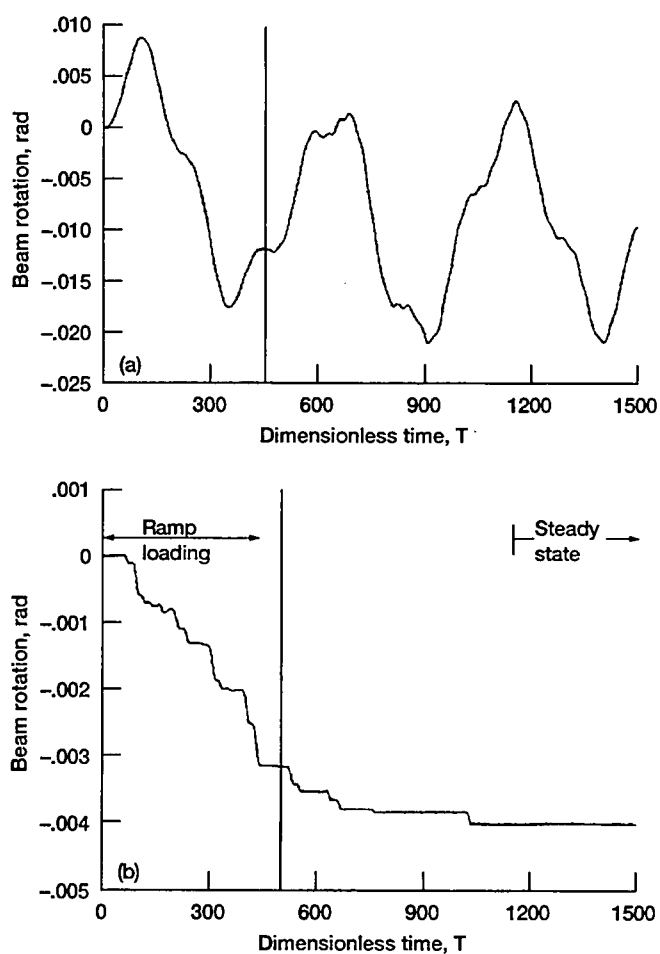
Figure 3.17.—Effect of friction on balance beam rotation. (a) Without friction. (b) With friction.
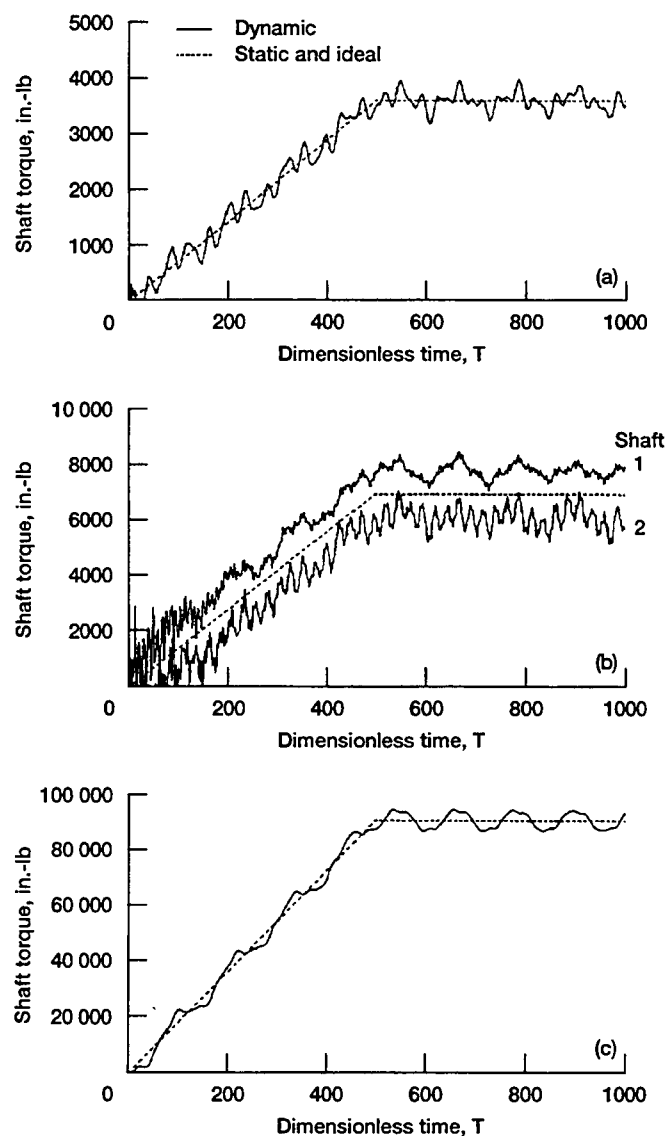
Figure 3.18.—Shaft torques with assembly error present. (a) Input shaft. (b) Compound shafts. (c) Output shafts.

58
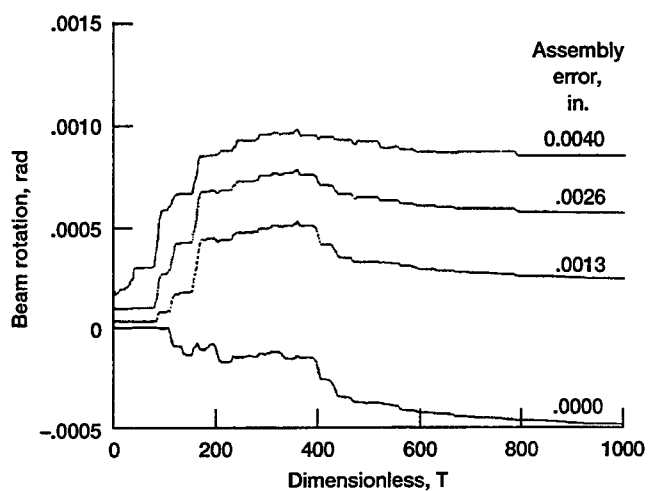
Figure 3.19.—Effect of assembly error on balance beam rotation.
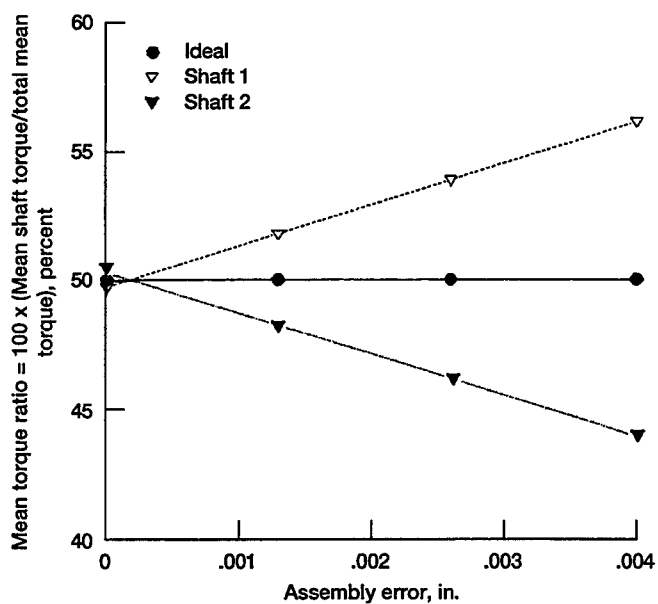
Figure 3.20.—Effect of assembly error on balance beam rotation.
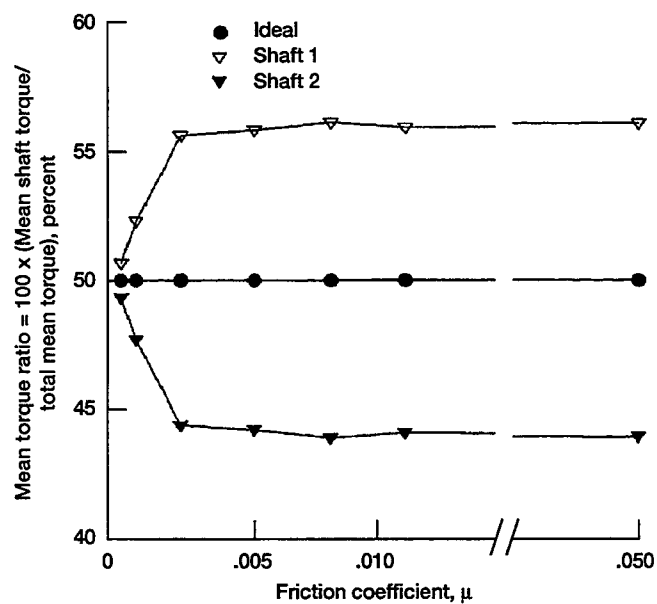
Figure 3.21.—Effect of friction on torque sharing.

Figure 3.23.—Dynamic total mesh deformation and components for helical mesh. (Note: positive deformation yields compression.)
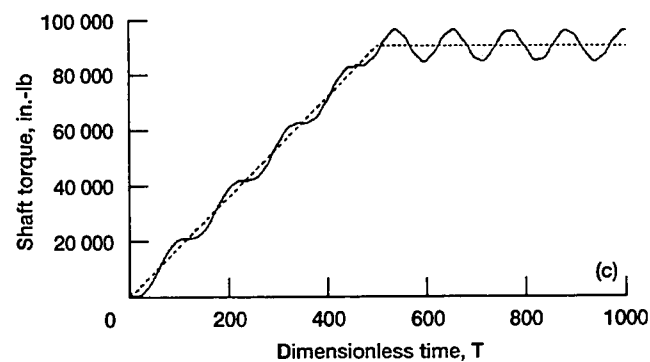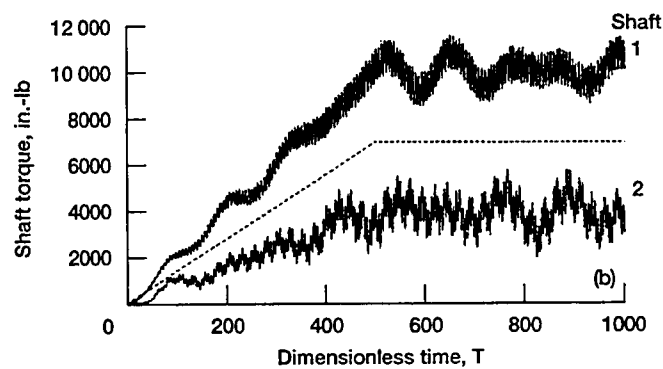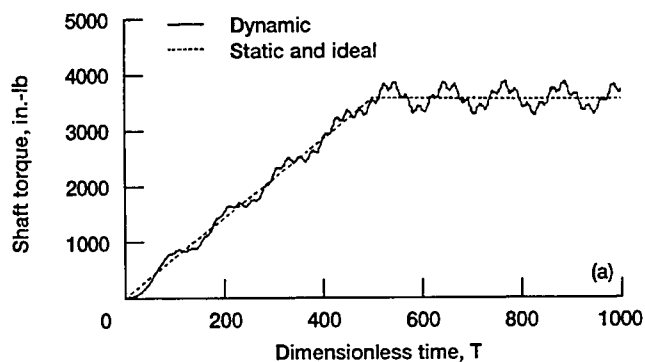
Figure 3.22.—Shaft torques with very stiff bearing supports. (a) Input shaft. (b) Compound shafts. (c) Output shaft.
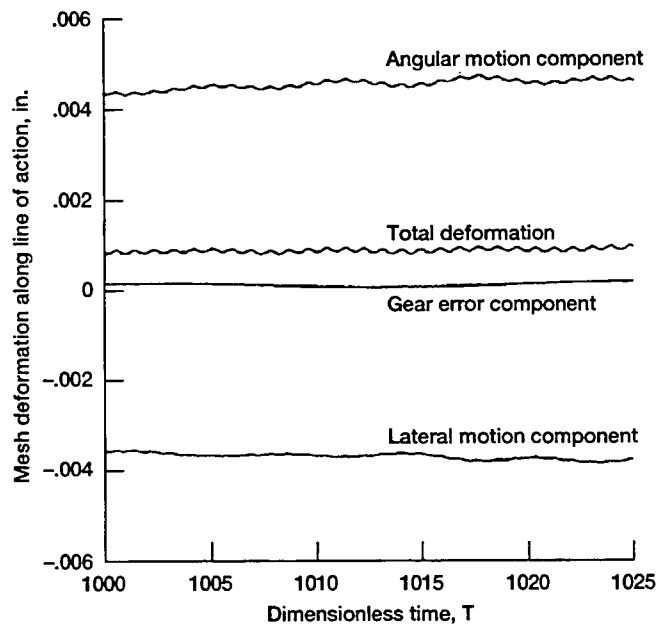
Figure 3.24.—Dynamic total mesh deformation and components for spur mesh. (Note: positive deformation yields compression.)

60
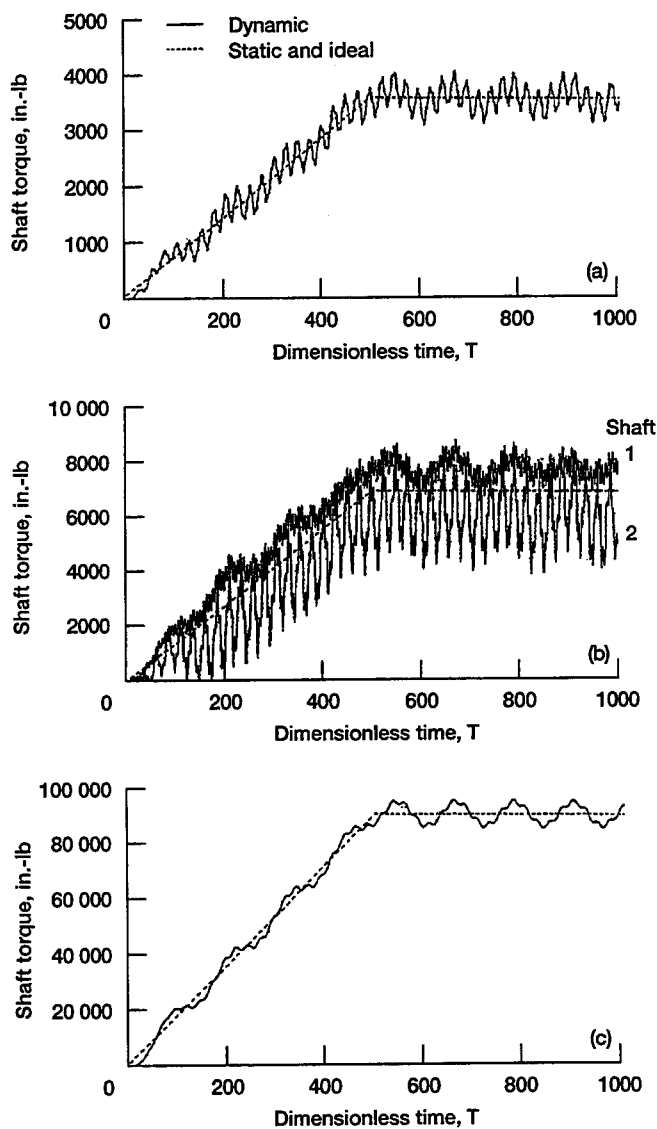
Figure 3.25.—Shaft torques with large total composite gear errors. (a) Input shaft. (b) Compound shafts. (c) Output shaft.
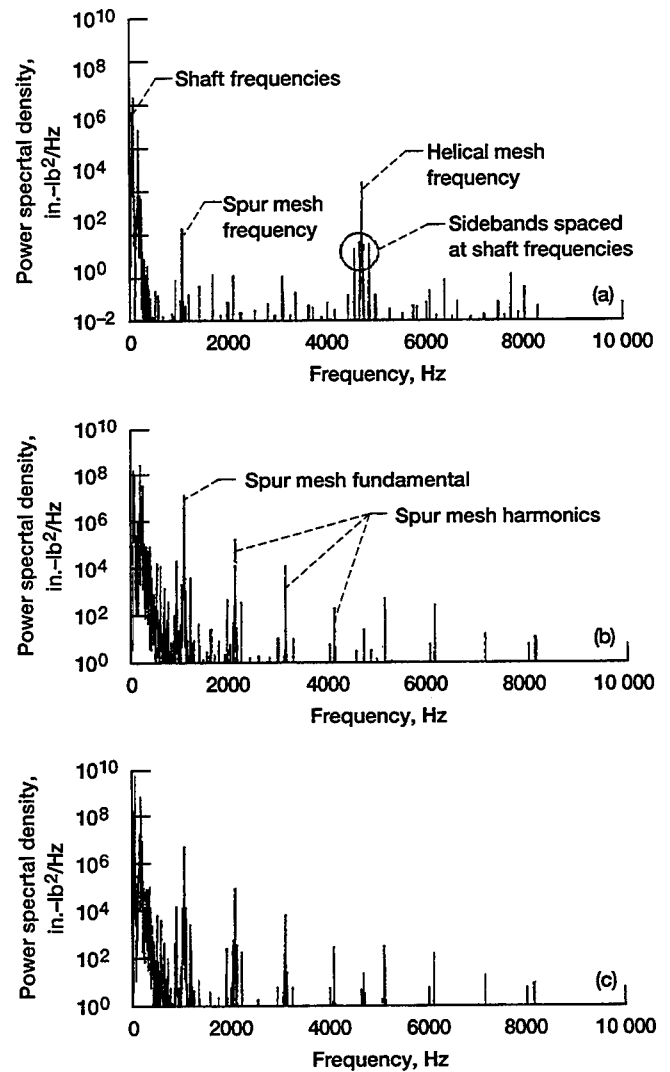
Figure 3.26.—Power spectral densities of shaft torques. (a) Input shaft. (b) Compound shaft 1. (c) Compound shaft 2.

61
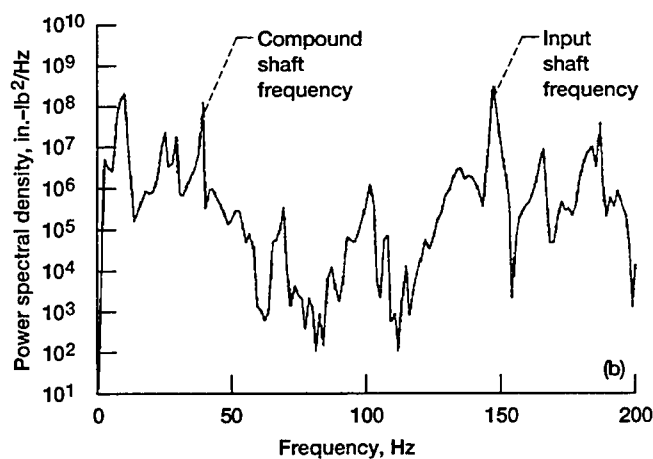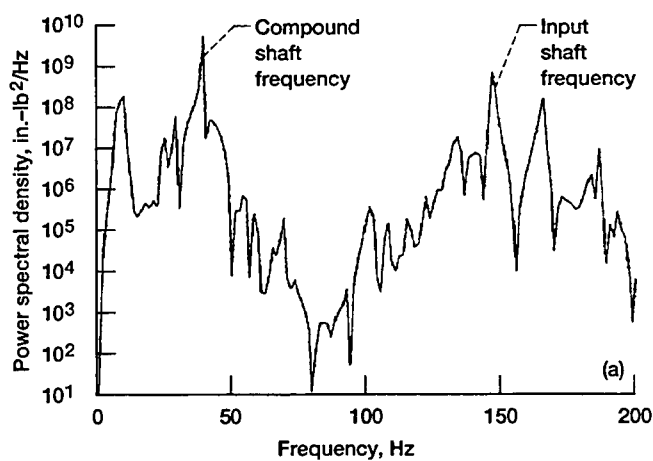
Figure 3.27.—Details of compound shaft torque spectra near shaft frequencies. (a) Compound shaft 2. (b) Compound shaft 1.
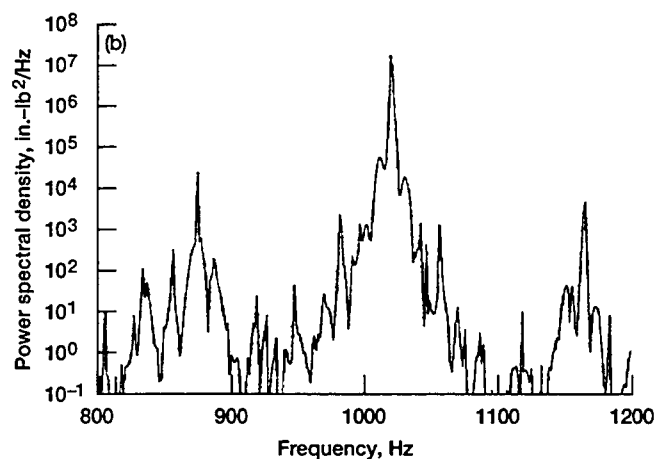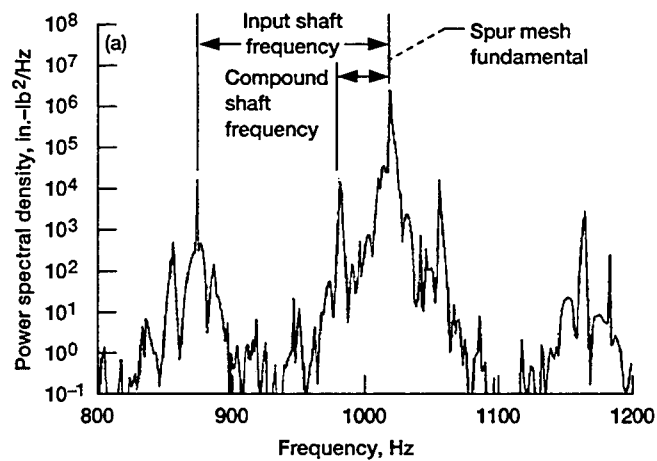
Figure 3.28.—Details of compound shaft torque spectra near spur mesh frequencies. (a) Compound shaft 2. (b) Compound shaft 1.
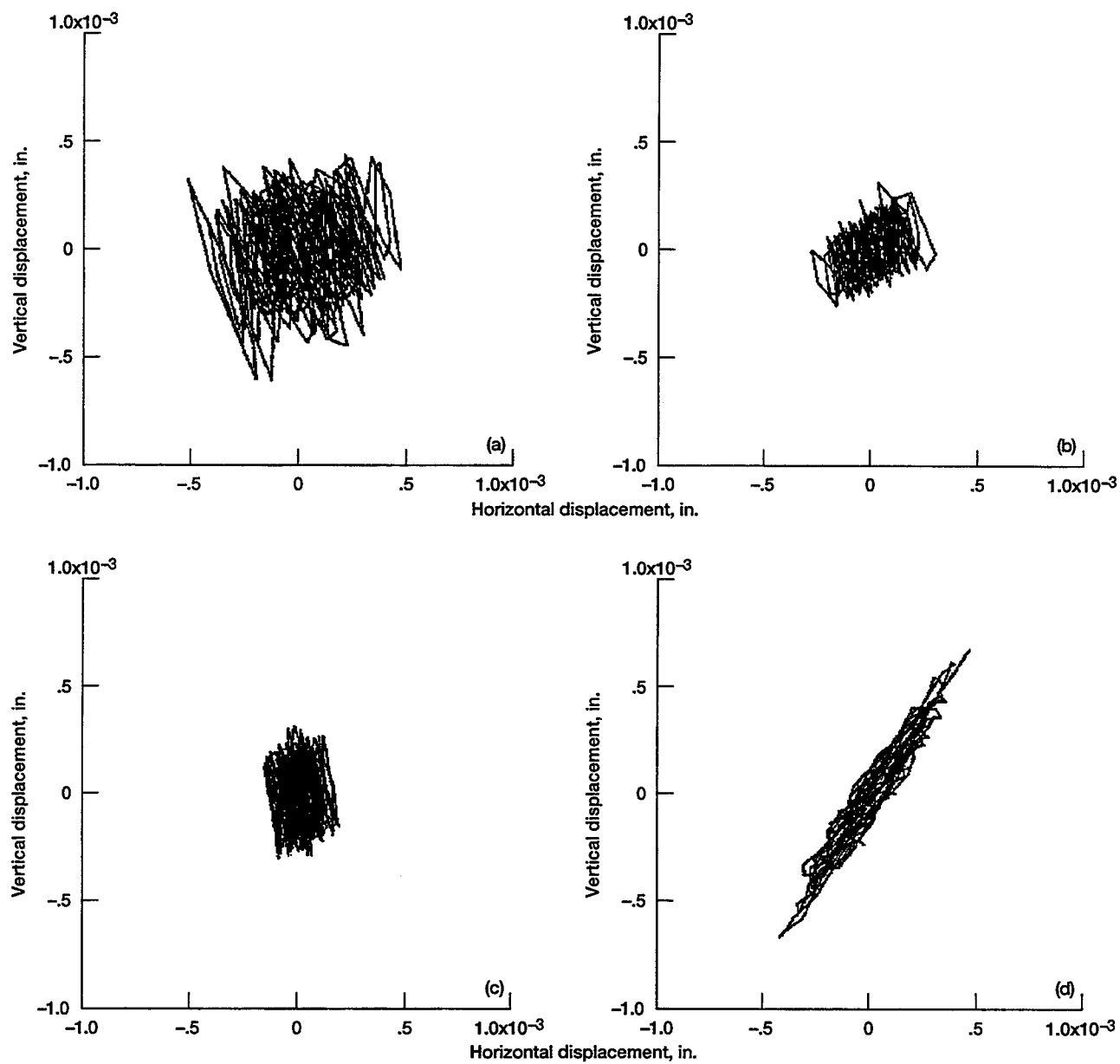
Figure 3.29.—Shaft orbits for large total composite gear errors. (a) Input pinion shaft. (b) Compound shaft 1. (c) Compound shaft 2. (d) Bull gear shaft.

63
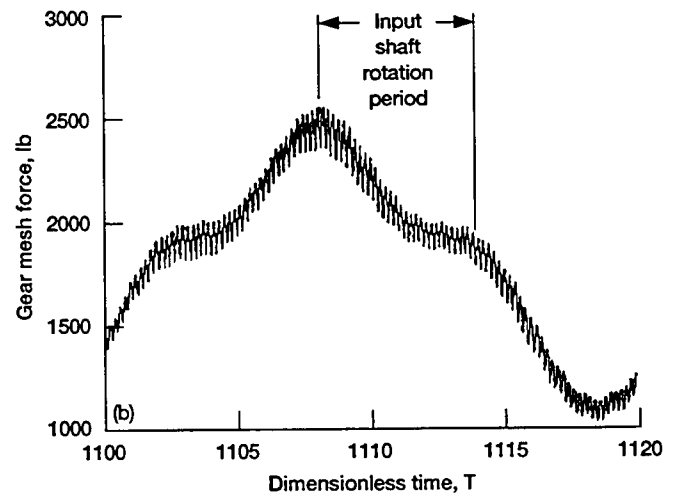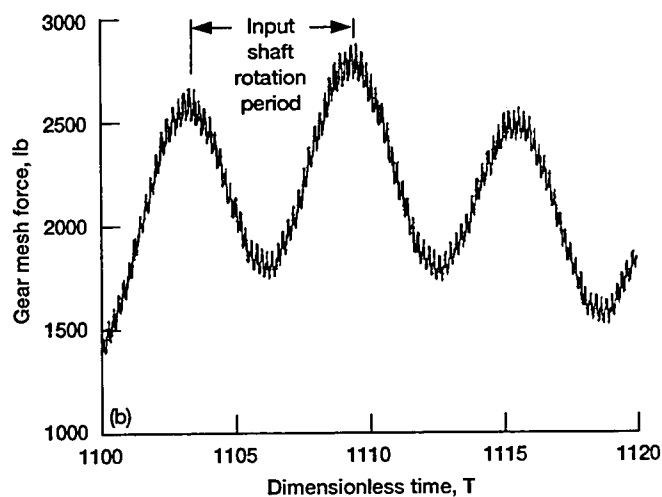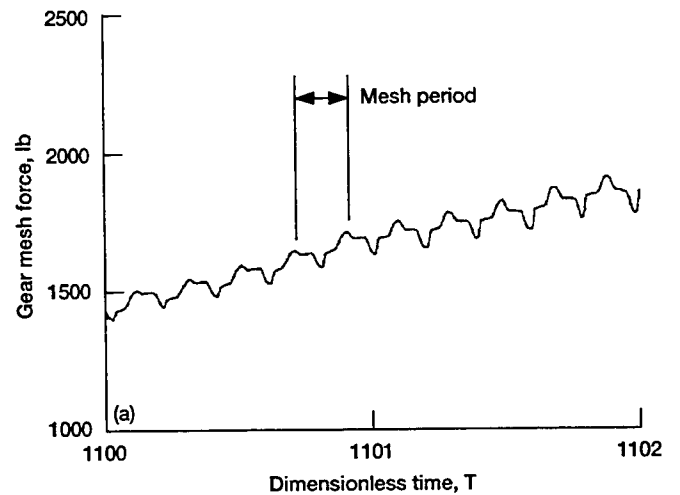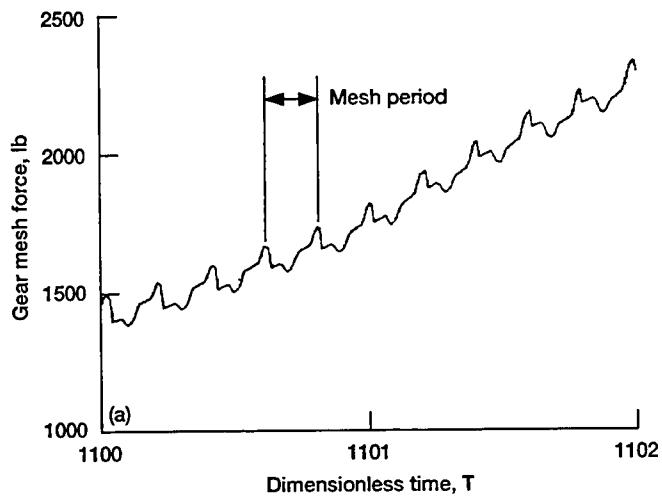
Figure 3.30.—Gear mesh forces for helical mesh 1. (a) Showing tooth frequencies. (b) Showing shaft frequencies.

Figure 3.31.—Gear mesh forces for helical mesh 2. (a) Showing tooth frequencies. (b) Showing shaft frequencies.
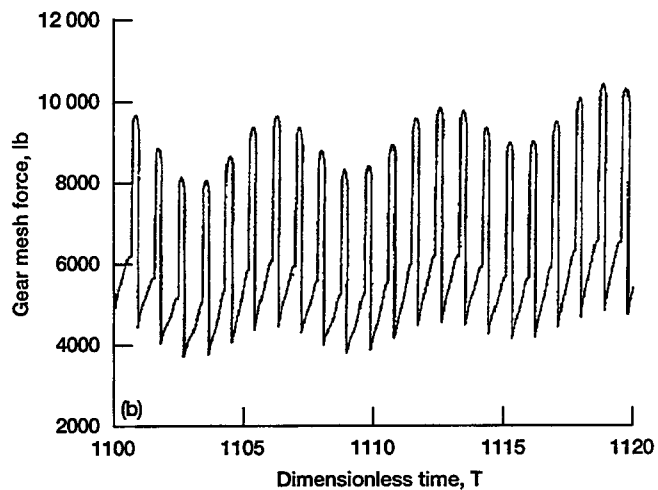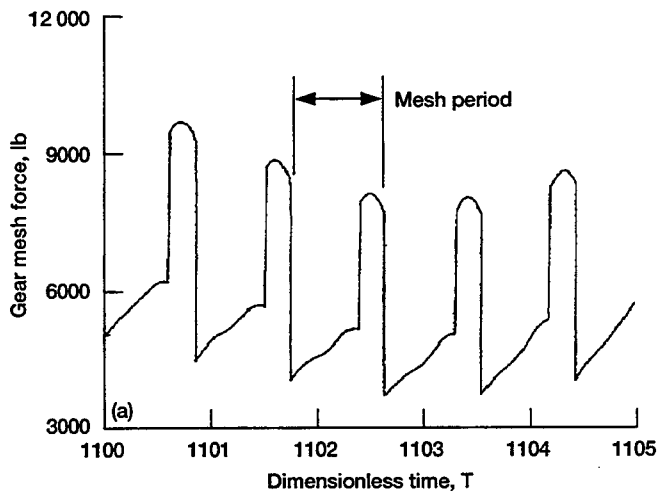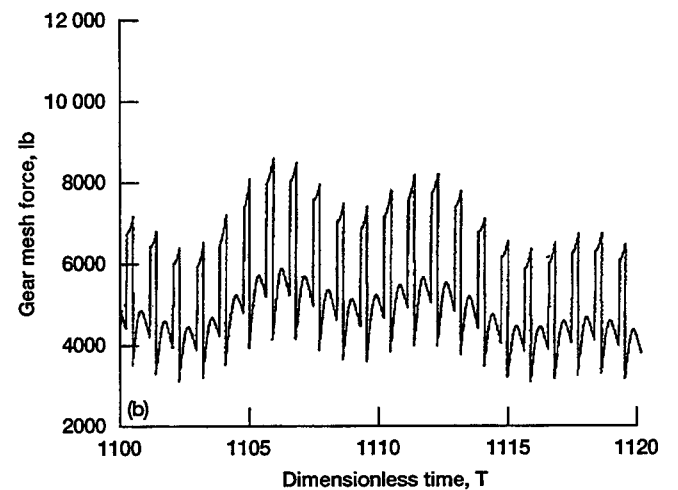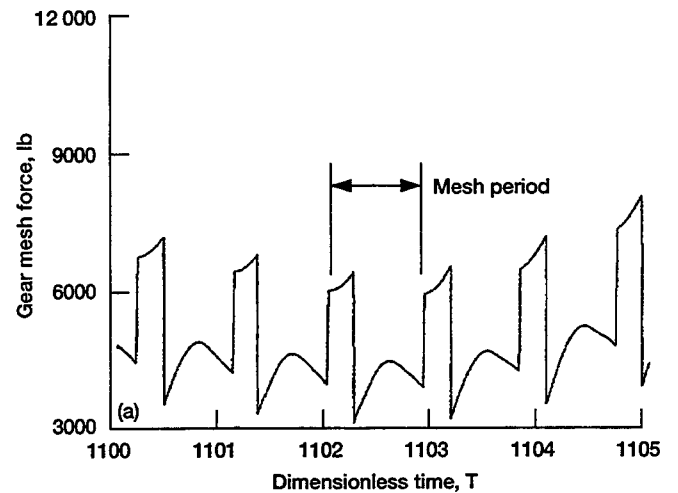
Figure 3.32.—Gear mesh forces for spur mesh 1. (a) Showing tooth frequencies. (b) Showing shaft frequencies.

Figure 3.33.—Gear mesh forces for spur mesh 2. (a) Showing tooth frequencies. (b) Showing shaft frequencies.
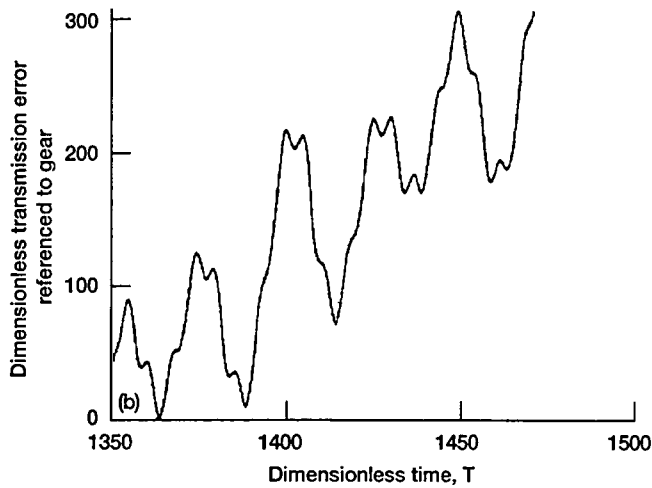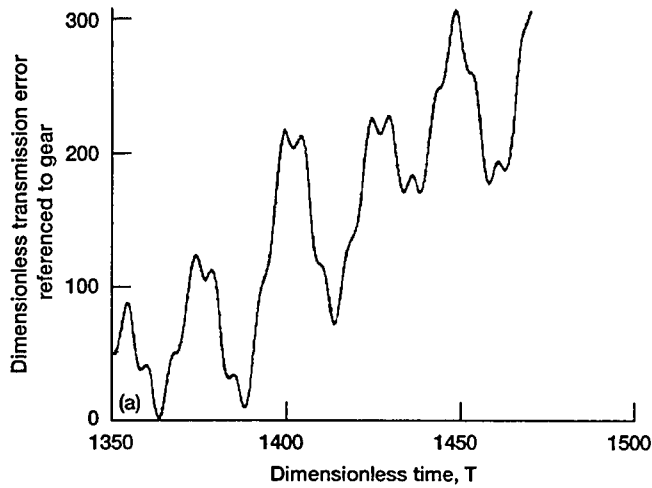
Figure 3.34.—Predicted transmission errors of helical meshes.
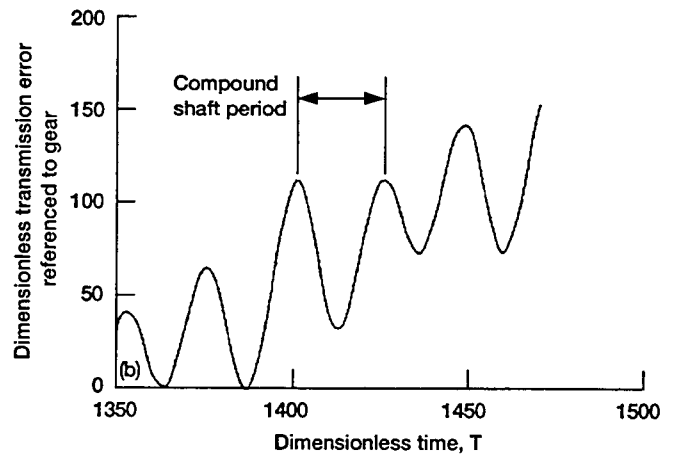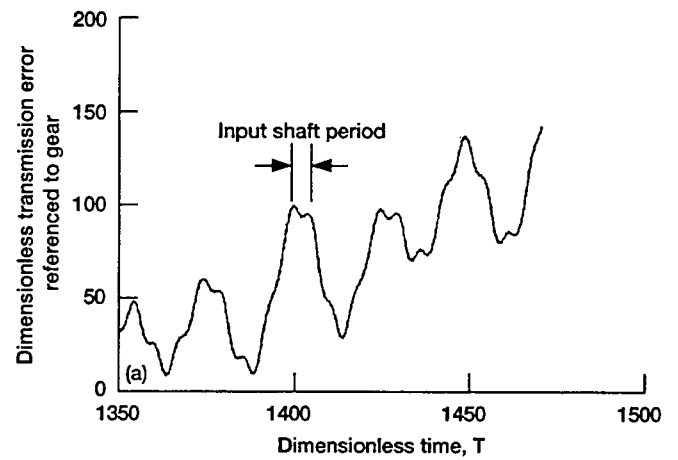(a) Helical gear 1. (b) Helical gear 2.

Figure 3.35.—Predicted transmission errors of spur meshes.
(a) Spur gear 1. (b) Spur gear 2.

66

REPORT DOCUMENTATION PAGE

Public reporting burden for this collection of information is estimated to average 1 hour per response, including the time for reviewing instructions, searching existing data sources, gathering and maintaining the data needed, and completing and reviewing the collection of information. Send comments regarding this burden estimate or any other aspect of this collection of information, including suggestions for reducing this burden, to Washington Headquarters Services, Directorate for Information Operations and Reports, 1215 Jefferson Davis Highway, Suite 1204, Arlington, VA 22202-4302, and to the Office of Management and Budget, Paperwork Reduction Project (0704-0188), Washington, DC 20503.

1. AGENCY USE ONLY (Leave blank)	2. REPORT DATE June 1994	3. REPORT TYPE AND DATES COVERED Technical Memorandum

4. TITLE AND SUBTITLE

Dynamics of a Split Torque Helicopter Transmission

5. FUNDING NUMBERS

WU–505–62–10
1L162211A47A

6. AUTHOR(S)

Timothy L. Krantz

7. PERFORMING ORGANIZATION NAME(S) AND ADDRESS(ES)

NASA Lewis Research Center
Cleveland, Ohio 44135–3191
and
Vehicle Propulsion Directorate
U.S. Army Research Laboratory
Cleveland, Ohio 44135–3191

8. PERFORMING ORGANIZATION REPORT NUMBER

E–7881

9. SPONSORING/MONITORING AGENCY NAME(S) AND ADDRESS(ES)

National Aeronautics and Space Administration
Washington, D.C. 20546–0001
and
U.S. Army Research Laboratory
Adelphi, Maryland 20783–1145

10. SPONSORING/MONITORING AGENCY REPORT NUMBER

NASA TM–106410
ARL–TR–291

11. SUPPLEMENTARY NOTES

This report was submitted as a thesis in partial fulfillment of the requirements for the degree Master of Science and Mechanical Engineering to Cleveland State University, Cleveland, Ohio 44115. Responsible person, Timothy L. Krantz, organization code 0300, (216) 433–3580.

12a. DISTRIBUTION/AVAILABILITY STATEMENT

Unclassified - Unlimited
Subject Category 37

12b. DISTRIBUTION CODE

13. ABSTRACT (Maximum 200 words)

Split torque designs, proposed as alternatives to traditional planetary designs for helicopter main rotor transmissions, can save weight and be more reliable than traditional designs. This report presents the results of an analytical study of the system dynamics and performance of a split torque gearbox that uses a balance beam mechanism for load sharing. The Lagrange method was applied to develop a system of equations of motion. The mathematical model includes time-varying gear mesh stiffness, friction, and manufacturing errors. Cornell's method for calculating the stiffness of spur gear teeth was extended and applied to helical gears. The phenomenon of sidebands spaced at shaft frequencies about gear mesh fundamental frequencies was simulated by modeling total composite gear errors as sinusoid functions. Although the gearbox has symmetric geometry, the loads and motions of the two power paths differ. Friction must be considered to properly evaluate the balance beam mechanism. For the design studied, the balance beam is not an effective device for load sharing unless the coefficient of friction is less than 0.003. The complete system stiffness as represented by the stiffness matrix used in this analysis must be considered to precisely determine the optimal tooth indexing position.

14. SUBJECT TERMS Gears; Transmissions; Vibrations; Helicopter transmissions	15. NUMBER OF PAGES 69
	16. PRICE CODE A04

17. SECURITY CLASSIFICATION OF REPORT Unclassified	18. SECURITY CLASSIFICATION OF THIS PAGE Unclassified	19. SECURITY CLASSIFICATION OF ABSTRACT Unclassified	20. LIMITATION OF ABSTRACT